Global fits in the Georgi-Machacek model

Cheng-Wei Chiang,[1,2,*] Giovanna Cottin,[1,†] and Otto Eberhardt[3,‡]
[1]*Department of Physics, National Taiwan University, Taipei 10617, Taiwan*
[2]*Institute of Physics, Academia Sinica, Taipei 11529, Taiwan*
[3]*IFIC, Universitat de València—Consejo Superior de Investigaciones Científicas, Apartado Correus 22085, E-46071 València, Spain*

(Received 19 November 2018; published 2 January 2019)

Off the beaten track of scalar singlet and doublet extensions of the Standard Model, triplets combine an interesting LHC phenomenology with an explanation for neutrino masses. The Georgi-Machacek model falls into this category, but it has never been fully explored in a global fit. We use the `HEPfit` package to combine recent experimental Higgs data with theoretical constraints and obtain strong limits on the mixing angles and mass differences between the heavy new scalars as well as their decay widths. We also find that the current signal strength measurements allow for a Higgs to vector boson coupling with an opposite sign to the Standard Model, but this possibility can be ruled out by the lack of direct evidence for heavy Higgs states. For these hypothetical particles, we identify the dominant decay channels and extract bounds on their branching ratios from the global fit, which can be used to single out the decay patterns relevant for the experimental searches.

DOI: 10.1103/PhysRevD.99.015001

I. INTRODUCTION

The discovery of a new scalar resonance at the LHC [1,2], consistent with the Higgs boson of the Standard Model (SM), confirms its particle content. Still several experimental observations, such as data on neutrino oscillations [3], beg for new physics explanations, whose effects are actively being looked for by the LHC experiments.

Among the well-motivated directions for new physics beyond the SM is the presence of an extended Higgs sector, which can lead to richer Higgs phenomenology at colliders. One possibility is the existence of additional Higgs triplet representations of $SU(2)$, in which neutrino masses can arise from the interaction of the SM Higgs doublet with the triplet field, that acquires a vacuum expectation value (VEV) v_Δ after electroweak symmetry breakdown (EWSB) [4,5]. Particularly in order to avoid conflicts with the electroweak ρ parameter [3], the Georgi-Machacek (GM) model [6,7] adds one complex and one real scalar triplet in a way that ensures custodial $SU(2)_V$ symmetry is preserved in the scalar potential after the EWSB. The model predicts the existence of several Higgs multiplets, whose mass eigenstates form a quintet (H_5), one triplet (H_3) and two singlets (H_1 and h) under the custodial symmetry. In this work, we denote the 125-GeV Higgs boson by h.

The rich Higgs particle spectrum and associated attractive phenomenology deserve in-depth studies, as it is of crucial importance to understand to which extent there is still room for new physics in the Higgs sector. Notably, if v_Δ is sufficiently large, we can have enhanced couplings between the SM-like Higgs boson and the weak gauge bosons. For example, $\kappa_W = 1.28^{+0.18}_{-0.17}$ is reported in a recent measurement by the CMS Collaboration [8], giving a hint for us to consider a Higgs sector with larger field representations [9,10]. The GM model serves as a minimal model with this feature. Modifications to the SM-like Higgs couplings with other particles can be probed by precise determination of the Higgs signal strengths at the LHC. Aside from loop-mediated processes, such data can constrain v_Δ and the mixing angle between the singlets α without the need to specify the heavy Higgs masses. In view of expected high precision in determining the Higgs couplings to other SM particles, Refs. [11,12] recently even computed the renormalized κ factors, defined to be Higgs couplings in the model normalized to their corresponding SM values, at the one-loop level. Since H_1 and h are related via an orthogonal rotation, these signal strengths also provide significant constraints on the couplings of H_1 to SM particles.

Earlier studies had shown various collider constraints on the parameter space of the GM model [10,13–19]. In Ref. [17], for example, it was shown that after considering

*chengwei@phys.ntu.edu.tw
†gcottin@phys.ntu.edu.tw
‡otto.eberhardt@ific.uv.es

theoretical bounds (namely, the stability of the potential and perturbative unitarity at tree level), the LHC Higgs signal strengths, together with electroweak precision observables, a favored region in the (v_Δ, α) plane is chosen by the data.

In this work, we go beyond the existing literature by performing global parameter fits in the GM model, including up-to-date experimental results from run 1 and run 2 of the LHC, by making use of the `HEPfit` open-source package [20]. This approach is in stark contrast to studies that only examine specific benchmark scenarios (that may miss interesting possibilities), as all the model parameters are varied simultaneously in the fits and a model likelihood is obtained. The package also allows the possibility to identify which of the experimental data impose most stringent bounds.

This paper is organized as follows. We start with a brief review of the GM model in Sec. II. A short overview over the `HEPfit` package can be found in Sec. III. Theoretical constraints on the scalar potential stability and perturbative unitarity at tree level are included in our fits as described in Sec. IV A. We then consider all available experimental data on Higgs boson signal strengths in Sec. IV B, including the $\gamma\gamma$ and the $Z\gamma$ modes, thus extending the considerations in Ref. [17]. Constraints from 80 heavy Higgs direct searches at the LHC are described in Sec. IV C. They are included in our Bayesian analysis and greatly extend the amount of constraints analyzed in previous works [14,16,17]. Combined results of the fits and discussions are presented in Sec. V. We close the paper with a summary of our findings in Sec. VI.

II. THE GEORGI-MACHACEK MODEL

In the GM model [6,7], $SU(2)$-triplet complex scalar χ and real scalar ξ are added to the SM particle content. Assuming that the custodial symmetry is preserved at tree level, we can write the SM doublet and new triplet scalar fields as a bidoublet and a bitriplet, respectively,

$$\Phi = \begin{pmatrix} (\phi^0)^* & \phi^+ \\ -(\phi^+)^* & \phi^0 \end{pmatrix},$$
$$\Delta = \begin{pmatrix} (\chi^0)^* & \xi^+ & \chi^{++} \\ -(\chi^+)^* & \xi^0 & \chi^+ \\ (\chi^{++})^* & -(\xi^+)^* & \chi^0 \end{pmatrix}.$$

After EWSB, the scalar fields have the VEVs given by

$$\langle \Phi \rangle = \frac{v_\Phi}{\sqrt{2}} \mathbb{1}_{2\times 2} \quad \text{and} \quad \langle \Delta \rangle = v_\Delta \mathbb{1}_{3\times 3}. \tag{1}$$

Using the above-defined fields, the scalar potential reads

$$V(\Phi,\Delta) = \frac{1}{2} m_\Phi^2 \mathrm{tr}[\Phi^\dagger\Phi] + \frac{1}{2} m_\Delta^2 \mathrm{tr}[\Delta^\dagger\Delta] + \lambda_1 (\mathrm{tr}[\Phi^\dagger\Phi])^2 + \lambda_2 (\mathrm{tr}[\Delta^\dagger\Delta])^2 + \lambda_3 \mathrm{tr}[(\Delta^\dagger\Delta)^2] + \lambda_4 \mathrm{tr}[\Phi^\dagger\Phi]\mathrm{tr}[\Delta^\dagger\Delta]$$
$$+ \lambda_5 \mathrm{tr}\left[\Phi^\dagger \frac{\sigma^a}{2} \Phi \frac{\sigma^b}{2}\right] \mathrm{tr}[\Delta^\dagger T^a \Delta T^b] + \mu_1 \mathrm{tr}\left[\Phi^\dagger \frac{\sigma^a}{2} \Phi \frac{\sigma^b}{2}\right] (P^\dagger \Delta P)_{ab} + \mu_2 \mathrm{tr}[\Delta^\dagger T^a \Delta T^b](P^\dagger \Delta P)_{ab}, \tag{2}$$

where σ^a are the Pauli matrices, T^a are the 3×3 matrix representation of the $SU(2)$ generators, and the similarity transformation relating the $SU(2)$ generators in the triplet and adjoint representations is given by

$$P = \frac{1}{\sqrt{2}} \begin{pmatrix} -1 & i & 0 \\ 0 & 0 & \sqrt{2} \\ 1 & i & 0 \end{pmatrix}.$$

Note that the triplet VEV is induced by the SM EWSB via the μ_1 interaction.

Under the custodial $SU(2)_V$ symmetry, the physical eigenstates can be written as a quintet $H_5 = (H_5^{++}, H_5^+, H_5^0, H_5^-, H_5^{--})^T$ with mass m_5, a triplet $H_3 = (H_3^+, H_3^0, H_3^-)^T$ with mass m_3 and two scalar singlets H_1 and h, of which the former has the mass m_1 and the latter is identified with the 125-GeV scalar boson found at the LHC. The relations between the physical fields and the original fields can be found in, for example, Ref. [13]. Rotating from the original basis to the mass basis involves two mixing angles α and β, where α diagonalizes the singlet subspace and $\tan\beta \equiv v_\Phi/(2\sqrt{2}v_\Delta)$ is used in the diagonalization of the Goldstone modes and the physical triplet states. In the limit of custodial symmetry, the states in each of the above-mentioned representations are degenerate in mass. An $\mathcal{O}(100)$ MeV mass splitting is expected among the states within the same representation because of custodial symmetry breaking by hypercharge interactions. In this article, we assume that h is the lightest scalar boson in the GM Higgs spectrum.

We list a few remarkable features of the GM model here. First, the hWW and hZZ couplings can be larger than the SM values at tree level. This does not happen in models extended with only singlet and/or doublet scalars. This feature is resistant to loop corrections, as explicitly shown in Refs. [11,12] at the one-loop level. Second, the quintet Higgs bosons have couplings with the weak gauge bosons, while the triplet Higgs bosons do not. The triplet Higgs

bosons are thus said to be gauge phobic. On the other hand, the triplet Higgs bosons have couplings with SM fermions, while the quintet Higgs bosons do not. The latter are thus said to be fermiophobic. Finally, the H_5^0ZZ coupling divided by the H_5^0WW coupling is -2, while the corresponding ratios for h and H_1 are 1.

III. HEPfit

The open-source package HEPfit is a multipurpose tool to calculate many different high-energy physics observables and theory constraints in various models. It is interfaced with BAT [21] to perform Bayesian fits with Markov chain Monte Carlo simulations. Here, we present the first results from the implementation of the GM model into HEPfit. The global fit allows us to scrutinize this model with unprecedented precision, as it allows us to vary all GM parameters simultaneously, and thus guarantees that we do not miss important features when scanning over the parameter space. This method has also been used in the two-Higgs doublet model [22–24], and the GM implementation is partially based on the well-tested two-Higgs doublet model part of HEPfit in order to minimize possible sources of errors. We also cross-checked some benchmark points with the public code GMcalc[25]. At tree level we found agreement on all couplings. Concerning the scalar couplings to $\gamma\gamma$ and $Z\gamma$ we observe deviations due to the different implementation of higher-order corrections. Moreover, HEPfit does not contain the one-loop decays $H_{3,5}^+ \to W^+\gamma$.

In our fits, we fix $m_h = 125.09$ GeV [26] and $v = \sqrt{v_\Phi^2 + 8v_\Delta^2} \approx 246$ GeV and all other SM parameters to their best-fit values [27]. We use the following prior ranges for the remaining GM parameters:

$$\begin{aligned} 150\ \text{GeV} \le m_1, m_3, m_5 \le 1100\ \text{GeV}, \\ 0\ \text{GeV} \le v_\Delta \le 86\ \text{GeV}, \\ -90° \le \alpha \le 90°, \\ -1500\ \text{GeV} \le \mu_1, \mu_2 \le 1500\ \text{GeV}, \end{aligned}$$

where the masses m_1, m_3, and m_5 of the H_1, H_3, and H_5 bosons, respectively, are chosen to be heavier than the 125-GeV Higgs and lighter than 1.1 TeV, as we want to cover the ranges that are interesting for the LHC searches of heavy scalars. Accordingly, we also limit the absolute values of the trilinear couplings μ_1 and μ_2 to be below 1.5 TeV.

Concerning the heavy masses m_1, m_3 and m_5, our type of priors will depend on the set of constraints being used. For the direct searches, we will use flat mass priors, as the search limits depend on the masses linearly. As for the h signal strengths and the theory bounds, they depend on the squared masses. Therefore, we choose flat priors for m_1^2, m_3^2 and m_5^2 between $(150\ \text{GeV})^2$ and $(1100\ \text{GeV})^2$ in this case. In the global fit to all constraints, we apply both types of priors in two separate fits and overlay both fits in the figures and for the extraction of the limits. (See also Appendix B of Ref. [23] for the same procedure in two-Higgs doublet model fits.)

IV. FIT CONSTRAINTS

In this section, we list the theoretical and experimental constraints imposed on the GM model parameter space in this analysis.

A. Theory constraints

We take into account two different sets of theoretical constraints: stability of the scalar potential and perturbative unitarity, both at tree level. Stability of the electroweak vacuum is imposed by requiring that the scalar potential be bounded from below, which places restrictions on the λ quartic couplings. We implement the constraints from Sec. IV of Ref. [28].

Perturbative unitarity of the S matrix of two scalars to two scalars scattering processes forces additional restrictions on the quartic couplings. We implement all 17 constraints from the full S matrix described in Ref. [29]. Here we take the stronger limits that the real parts of the zeroth partial wave amplitudes have absolute values of less than $1/2$.

We note that the theoretical bounds implemented in this work are conservative. Perturbative unitarity can be broken in the GM model [30]. Also, the tree-level vacuum stability constraints can change once loop corrections are included [31]. Since the focus of this work is on LHC constraints, we keep a more relaxed analysis in terms of the allowed parameter space from the theory side, but this can be more restrictive.

While the theory constraints are defined in terms of the quartic couplings of the scalar potential in Eq. (2), the following experimental bounds constrain the physical masses and the couplings of the scalars.

B. Higgs signal strengths

For the signal strengths computation, the predicted SM Higgs production cross section σ and total decay width Γ are dressed with scale factors. For the production modes $i =$ ggF, VBF, Wh, Zh, tth and the decay modes $f = ZZ, WW, \gamma\gamma, Z\gamma, \tau\tau, \mu\mu, b\bar{b}$, we define r_i and r_f to be, respectively, the ratios of the production cross section σ_i and the decay width Γ_f with respect to their corresponding SM values. Therefore, the production cross section times the branching ratio for a particular channel in the GM model is given by

TABLE I. Higgs signal strength inputs used in our fits. The Higgs decays are listed in separate columns, with the corresponding SM branching ratios given in the second line. In lines 3–12, we give all LHC and Tevatron references of the used signal strengths, ordered by production mechanism and $\sqrt{s}$. For the LHC, we indicate the share of Higgs production in pp collisions for each channel in the second column. The background colors of the table cells give an idea about how precise the strongest signal strength measurement for a particular production mechanism is at present: Green cells contain results with an uncertainty of less than 0.5 on μ, yellow cells have an uncertainty between 0.5 and 1, and red entries have not been measured with a precision smaller than 1 (see the text for more details). On the decays to $Z\gamma$ and $\mu\mu$, we only have information for pp production and assume the SM composition in the second column for them.

		$b\bar{b}$	WW	$\tau\tau$	ZZ	$\gamma\gamma$	$Z\gamma$	$\mu\mu$
SM Br		57.5%	21.6%	6.3%	2.7%	2.3‰	1.6‰	0.2‰
ggF_8	87.2%	…	[32, 33]	[34, 35]	[36, 37]	[38, 39]	[40, 41]	[26]
ggF_{13}	87.1%	…	[8, 42]	[43, 44]	[45–47]	[48, 49]	[50, 51]	[52, 53]
VBF_8	7.2%	…	[32, 33]	[34, 35]	[36, 37]	[38, 39]		
VBF_{13}	7.4%	[54, 55]	[8, 42]	[43, 44]	[45–47]	[48, 49]		
Vh_8	5.1%	[56, 57]	[33, 58]	[34, 35]	[36, 37]	[38, 39]		
Vh_{13}	4.4%	[59, 60]	[8, 61]	[44, 62]	[45–47]	[48, 49]		
tth_8	0.6%	[63, 64]	…	…	[36, 37]	[38, 39]		
tth_{13}	1.0%	[65–67]	[8, 68, 69]	[68, 69]	[45–47, 68, 69]	[48, 49]		
Vh_2		[70, 71]						
tth_2		[70]						

$0 < \hat{\sigma} < 0.5$ | $0.5 \leq \hat{\sigma} \leq 1.0$ | $\hat{\sigma} > 1.0$ $\quad (\hat{\sigma} = \sigma_{\min}/w)$

$$(\sigma_i \cdot \mathcal{B}_f)_{\mathrm{GM}} = (\sigma_i \cdot \mathcal{B}_f)_{\mathrm{SM}} \cdot r_i \cdot r_f \cdot \frac{\Gamma_{\mathrm{SM}}}{\Gamma_{\mathrm{GM}}}, \tag{3}$$

with Γ_{SM} and Γ_{GM} being the total widths of the Higgs boson in the SM and the GM model, respectively.

To quantify the deviation of the GM model from the SM, the signal strength of a process μ_i^f with the production channel i and the decay of h to an f final state is then defined as

$$\mu_i^f = \frac{r_i \cdot r_f}{\sum_{f'} r_{f'} \cdot \mathcal{B}_{\mathrm{SM}}(h \to f')}. \tag{4}$$

Each signal strength is computed in the narrow-width approximation and depends on the GM h couplings to all final states. The values for all couplings are cross-checked with the predictions in Ref. [25].

The experimental input values of the Higgs signal strengths are similar to the ones in Ref. [72], only that we updated some numbers after the ICHEP 2018. Instead of all 138 numerical signal strength inputs, we show in Table I the current sensitivity of the individual channels, indicated by the background colors. The quantity $\hat{\sigma}$ is the ratio of the smallest uncertainty of all individual measurements in one table cell ($\sigma_{\min}$) and the weight of the corresponding production mechanism (w). For instance, in Ref. [44], we can find that $\mu^{\tau\tau} = 1.11^{+0.34}_{-0.35}$ in their "VBF" category, so $\sigma_{\min} = 0.34$ here. Note that the categories do not consist of only one production mechanism, and thus the given value is no measurement of $\mu^{\tau\tau}_{\mathrm{VBF}}$. The admixture (weight) of VBF is only 57%, and so $\hat{\sigma} \approx 0.6$ in this case. We stress that $\hat{\sigma}$ depends on the *individual* measurements and not on the combination. It is only intended to give the reader a rough estimate of the achieved precision in every channel and should not be

understood as a quantitative statement. In the last two columns, we use the 8-TeV data from Refs. [40,41] ([26]) and the 13-TeV results from Refs. [50,51] ([52,53]) for the $Z\gamma$ ($\mu\mu$) final state, since the only information about the initial state is the inclusive pp production rather than individual channels.

C. Searches for heavy Higgs particles

We consider a large variety of direct searches for heavy resonances performed by the ATLAS and CMS Collaborations in run 1 and run 2 of the LHC. Tables II–V summarize the experimental searches to date which can have sensitivity to the neutral scalars H_1^0, H_3^0 and H_5^0 in the GM model. Tables II and III show all searches for a scalar resonance decaying into fermions or gauge bosons, and in Table IV we list the cases with decays including one or two Higgs bosons. In Table V, we list all searches for singly and doubly charged heavy scalars considered in our fits. Note that we are not sensitive in this model to the doubly charged Higgs searches in Refs. [135–137], where a 100% branching fraction to leptons is assumed and the decay of $H_5^{\pm\pm}$ to $W^\pm W^\pm$ is suppressed, a scenario quite contrary to what we are considering here. The ATLAS searches for a doubly charged Higgs in Refs. [138,139] can have sensitivity in the two-lepton and three-lepton signal regions and have been reinterpreted in the context of the Higgs triplet model [140] and GM model [16]. Also these limits are not applicable to our case due to the $\mathcal{B}(H^{\pm\pm} \to \ell^\pm \ell^\pm) = 100\%$ assumption, and, since in this work we are not formally recasting these searches, we choose not to include them in the fits.

TABLE II. Neutral heavy Higgs boson searches relevant for the GM scalars with fermionic final states. $\phi^0 = H_1^0, H_3^0$.

Label	Channel	Experiment	Mass range [TeV]	$\mathcal{L}$ [fb^{-1}]
A_{13t}^{tt}	$tt \to \phi^0 \to tt$	ATLAS [73]	[0.4;1]	36.1
A_{13b}^{tt}	$bb \to \phi^0 \to tt$	ATLAS [74]	[0.4;1]	13.2
C_{8b}^{bb}	$bb \to \phi^0 \to bb$	CMS [75]	[0.1;0.9]	19.7
C_{8}^{bb}	$gg \to \phi^0 \to bb$	CMS [76]	[0.33;1.2]	19.7
C_{13}^{bb}	$pp \to \phi^0 \to bb$	CMS [77]	[0.55;1.2]	2.69
C_{13b}^{bb}	$bb \to \phi^0 \to bb$	CMS [78]	[0.3;1.3]	35.7
$A_{8}^{\tau\tau}$	$gg \to \phi^0 \to \tau\tau$	ATLAS [79]	[0.09;1]	20
$C_{8}^{\tau\tau}$		CMS [80]	[0.09;1]	19.7
$A_{8b}^{\tau\tau}$	$bb \to \phi^0 \to \tau\tau$	ATLAS [79]	[0.09;1]	20
$C_{8b}^{\tau\tau}$		CMS [80]	[0.09;1]	19.7
$A_{13}^{\tau\tau}$	$gg \to \phi^0 \to \tau\tau$	ATLAS [81]	[0.2;2.25]	36.1
$C_{13}^{\tau\tau}$		CMS [82]	[0.09;3.2]	35.9
$A_{13b}^{\tau\tau}$	$bb \to \phi^0 \to \tau\tau$	ATLAS [81]	[0.2;2.25]	36.1
$C_{13b}^{\tau\tau}$		CMS [82]	[0.09;3.2]	35.9

The analyses in Tables II–V provide either model-independent 95% confidence level upper limits on the production cross-section times branching ratios, $\sigma \cdot \mathcal{B}$, for different production and decay modes, or they are quoted by $\sigma \cdot \mathcal{B}/(\sigma \cdot \mathcal{B})_{\rm SM}$ as a function of the resonance mass. If the experimental result includes the branching ratio into a specific final state in the upper limit, we write this channel using parentheses to combine particles which stem from a primary decay product. Whenever a secondary final state is given in square brackets, it means that we are quoting the limit on the primary final state measured through that particular secondary final state.

In order to assess which parts of the GM model parameter space are favored after imposing these constraints, we first calculate the theoretical production cross-section times branching ratio $\sigma \cdot \mathcal{B}$ for all modes. For the neutral H_1^0, H_3^0 and singly charged $H_3^\pm$ states, we calculate $\sigma \cdot \mathcal{B}$ taking inputs from the two-Higgs doublet model already implemented in `HEPfit` [22,23] and rescale it to the GM model. We make use of the cross-section tables computed in Refs. [22,23] and calculate all branching ratios taking inputs from the couplings defined in the Appendix of Ref. [141]. For the VBF production cross sections for $H_5^{\pm\pm}$, $H_5^\pm$, and H_5^0, we use the 8- and 13-TeV production cross-section tables from the LHC Higgs Cross-Section Working Group [142]. The remaining VH quintet production modes and pair production of doubly charged $H_5^{\pm\pm}$ are calculated with MadGraph5_aMC@NLOv2.6.1 [143] at the leading order, taking the spectrum of the model generated with GMcalc [25] as input. All the mentioned tables are interpolated linearly within `HEPfit`.

In order to compare a specific $\sigma \cdot \mathcal{B}$ (calculated in each case as above) with the experimental upper limit, we define a ratio for the theoretical value and the observed limit, to which we assign a Gaussian likelihood with zero central value, which is in agreement with the null results in the searches of heavy scalars so far. The corresponding standard deviation of the Gaussian likelihood is adjusted in a way that the value of 1 for this ratio can be excluded with a probability of 95%.

V. RESULTS

Here we show the impact of all the constraints considered on the GM model. We first discuss the effect of

TABLE III. Neutral heavy Higgs boson searches relevant for the GM scalars with vector boson final states. $\phi^0 = H_1^0, H_3^0, H_5^0$ and $\ell = e, \mu$.

Label	Channel	Experiment	Mass range [TeV]	$\mathcal{L}$ [fb^{-1}]
$A_8^{\gamma\gamma}$	$gg \to \phi^0 \to \gamma\gamma$	ATLAS [83]	[0.065;0.6]	20.3
$A_{13}^{\gamma\gamma}$	$pp \to \phi^0 \to \gamma\gamma$	ATLAS [84]	[0.2;2.7]	36.7
$C_{13}^{\gamma\gamma}$	$gg \to \phi^0 \to \gamma\gamma$	CMS [85]	[0.5;4]	35.9
$A_8^{Z\gamma}$	$pp \to \phi^0 \to Z\gamma \to (\ell\ell)\gamma$	ATLAS [86]	[0.2;1.6]	20.3
$C_8^{Z\gamma}$		CMS [87]	[0.2;1.2]	19.7
$A_{13}^{\ell\ell\gamma}$	$gg \to \phi^0 \to Z\gamma[\to (\ell\ell)\gamma]$	ATLAS [50]	[0.25;2.4]	36.1
$A_{13}^{qq\gamma}$	$gg \to \phi^0 \to Z\gamma[\to (qq)\gamma]$	ATLAS [88]	[1;6.8]	36.1
$C_{8+13}^{Z\gamma}$	$gg \to \phi^0 \to Z\gamma$	CMS [89]	[0.35;4]	35.9
A_8^{ZZ}	$gg \to \phi^0 \to ZZ$	ATLAS [90]	[0.14;1]	20.3
A_{8V}^{ZZ}	$VV \to \phi^0 \to ZZ$	ATLAS [90]	[0.14;1]	20.3
$A_{13}^{2\ell 2L}$	$gg \to \phi^0 \to ZZ[\to (\ell\ell)(\ell\ell,\nu\nu)]$	ATLAS [91]	[0.2;1.2]	36.1
$A_{13V}^{2\ell 2L}$	$VV \to \phi^0 \to ZZ[\to (\ell\ell)(\ell\ell,\nu\nu)]$	ATLAS [91]	[0.2;1.2]	36.1
A_{13}^{2L2q}	$gg \to \phi^0 \to ZZ[\to (\ell\ell,\nu\nu)(qq)]$	ATLAS [92]	[0.3;3]	36.1
A_{13V}^{2L2q}	$VV \to \phi^0 \to ZZ[\to (\ell\ell,\nu\nu)(qq)]$	ATLAS [92]	[0.3;3]	36.1
$C_{13}^{2\ell 2X}$	$pp \to \phi^0 \to ZZ[\to (\ell\ell)(qq,\nu\nu,\ell\ell)]$	CMS [93]	[0.13;3]	35.9
$C_{13}^{2q2\nu}$	$pp \to \phi^0 \to ZZ[\to (qq)(\nu\nu)]$	CMS [94]	[1;4]	35.9
A_8^{WW}	$gg \to \phi^0 \to WW$	ATLAS [95]	[0.3;1.5]	20.3
A_{8V}^{WW}	$VV \to \phi^0 \to WW$	ATLAS [95]	[0.3;1.5]	20.3
$A_{13}^{2(\ell\nu)}$	$gg \to \phi^0 \to WW[\to (e\nu)(\mu\nu)]$	ATLAS [96]	[0.25;4]	36.1
$A_{13V}^{2(\ell\nu)}$	$VV \to \phi^0 \to WW[\to (e\nu)(\mu\nu)]$	ATLAS [96]	[0.25;3]	36.1
$C_{13}^{2(\ell\nu)}$	$(gg{+}VV) \to \phi^0 \to WW \to (\ell\nu)(\ell\nu)$	CMS [97]	[0.2;1]	2.3
$A_{13}^{\ell\nu 2q}$	$gg \to \phi^0 \to WW[\to (\ell\nu)(qq)]$	ATLAS [98]	[0.3;3]	36.1
$A_{13V}^{\ell\nu 2q}$	$VV \to \phi^0 \to WW[\to (\ell\nu)(qq)]$	ATLAS [98]	[0.3;3]	36.1
$C_{13}^{\ell\nu 2q}$	$pp \to \phi^0 \to WW[\to (\ell\nu)(qq)]$	CMS [99]	[1;4.4]	35.9
C_8^{VV}	$pp \to \phi^0 \to VV$	CMS [100]	[0.145;1]	24.8

TABLE IV. Neutral heavy Higgs boson searches at the LHC relevant for the GM scalars with final states including Higgs bosons. $\phi^0 = H_1^0, H_3^0, H_5^0$, $\phi'^0 = H_1^0, H_3^0$, $V = W$, Z and $\ell = e$, μ.

Label	Channel	Experiment	Mass range [TeV]	$\mathcal{L}$ [fb^{-1}]
A_8^{hh}	$gg \to H_1^0 \to hh$	ATLAS [101]	[0.26;1]	20.3
C_8^{4b}	$pp \to H_1^0 \to hh \to (bb)(bb)$	CMS [102]	[0.27;1.1]	17.9
$C_8^{2\gamma 2b}$	$pp \to H_1^0 \to hh \to (bb)(\gamma\gamma)$	CMS [103]	[0.260;1.1]	19.7
$C_{8g}^{2b2\tau}$	$gg \to H_1^0 \to hh \to (bb)(\tau\tau)$	CMS [104]	[0.26;0.35]	19.7
$C_8^{2b2\tau}$	$pp \to H_1^0 \to hh[\to (bb)(\tau\tau)]$	CMS [105]	[0.35;1]	18.3
A_{13}^{4b}	$pp \to H_1^0 \to hh \to (bb)(bb)$	ATLAS [106]	[0.26;3]	36.1
C_{13}^{4b}		CMS [107]	[0.26;1.2]	35.9
$A_{13}^{2\gamma 2b}$	$pp \to H_1^0 \to hh[\to (bb)(\gamma\gamma)]$	ATLAS [108]	[0.26;1]	36.1
$C_{13}^{2\gamma 2b}$	$pp \to H_1^0 \to hh \to (bb)(\gamma\gamma)$	CMS [109]	[0.25;0.9]	35.9
$A_{13}^{2b2\tau}$	$pp \to H_1^0 \to hh \to (bb)(\tau\tau)$	ATLAS [110]	[0.26;1]	36.1
$C_{13,1}^{2b2\tau}$		CMS [111]	[0.25;0.9]	35.9
$C_{13,2}^{2b2\tau}$	$pp \to H_1^0 \to hh[\to (bb)(\tau\tau)]$	CMS [112]	[0.9;4]	35.9
C_{13}^{2b2V}	$pp \to H_1^0 \to hh \to (bb)(VV \to \ell\nu\ell\nu)$	CMS [113]	[0.26;0.9]	35.9
$A_{13}^{2\gamma 2W}$	$gg \to H_1^0 \to hh \to (\gamma\gamma)(WW)$	ATLAS [114]	[0.26;0.5]	36.1
A_8^{bbZ}	$gg \to H_3^0 \to hZ \to (bb)Z$	ATLAS [115]	[0.22;1]	20.3
$C_8^{2b2\ell}$	$gg \to H_3^0 \to hZ \to (bb)(\ell\ell)$	CMS [116]	[0.225;0.6]	19.7
$A_8^{\tau\tau Z}$	$gg \to H_3^0 \to hZ \to (\tau\tau)Z$	ATLAS [115]	[0.22;1]	20.3
$C_8^{2\tau 2\ell}$	$gg \to H_3^0 \to hZ \to (\tau\tau)(\ell\ell)$	CMS [104]	[0.22;0.35]	19.7
A_{13}^{bbZ}	$gg \to H_3^0 \to hZ \to (bb)Z$	ATLAS [117]	[0.2;2]	36.1
$C_{13,1}^{bbZ}$		CMS [118]	[0.22;0.8]	35.9
$C_{13,2}^{bbZ}$		CMS [119]	[0.8;2]	35.9
A_{13b}^{bbZ}	$bb \to H_3^0 \to hZ \to (bb)Z$	ATLAS [117]	[0.2;2]	36.1
$C_{13b,1}^{bbZ}$		CMS [118]	[0.22;0.8]	35.9
$C_{13b,2}^{bbZ}$		CMS [119]	[0.8;2]	35.9
$C_8^{\phi Z}$	$pp \to \phi^0 \to \phi^{0\prime} Z \to (bb)(\ell\ell)$	CMS [120]	[0.13;1]	19.8
$A_{13}^{\phi Z}$	$gg \to H_3^0 \to H_1^0 Z \to (bb)Z$	ATLAS [121]	[0.13;0.8]	36.1
$A_{13b}^{\phi Z}$	$bb \to H_3^0 \to H_1^0 Z \to (bb)Z$	ATLAS [121]	[0.13;0.8]	36.1

TABLE V. Charged heavy Higgs boson searches at the LHC relevant for the singly and doubly charged scalars in the GM model. Again, $V = W$, Z and $\ell = e$, μ.

Label	Channel	Experiment	Mass range [TeV]	$\mathcal{L}$ [fb^{-1}]
$A_8^{\tau\nu}$	$pp \to H_3^{\pm} \to \tau^{\pm}\nu$	ATLAS [122]	[0.18;1]	19.5
$C_8^{\tau\nu}$	$pp \to H_3^{+} \to \tau^{+}\nu$	CMS [123]	[0.18;0.6]	19.7
$A_{13}^{\tau\nu}$	$pp \to H_3^{\pm} \to \tau^{\pm}\nu$	ATLAS [124]	[0.15;2]	36.1
$C_{13}^{\tau\nu}$		CMS [125]	[0.18;3]	12.9
A_8^{tb}	$pp \to H_3^{\pm} \to tb$	ATLAS [126]	[0.2;0.6]	20.3
C_8^{tb}	$pp \to H_3^{+} \to t\bar{b}$	CMS [123]	[0.18;0.6]	19.7
A_{13}^{tb}	$pp \to H_3^{\pm} \to tb$	ATLAS [127]	[0.2;2]	36.1
A_8^{WZ}	$WZ \to H_5^{\pm} \to WZ[\to (qq)(\ell\ell)]$	ATLAS [128]	[0.2;1]	20.3
A_{13}^{WZ}	$WZ \to H_5^{\pm} \to WZ[\to (\ell\nu)(\ell\ell)]$	ATLAS [129]	[0.2;0.9]	36.1
$C_{13,1}^{WZ}$		CMS [130]	[0.2;0.3]	15.2
$C_{13,2}^{WZ}$		CMS [131]	[0.3;2]	35.9
A_{13}^{4W}	$pp \to H_5^{\pm\pm}H_5^{\mp\mp} \to (W^{\pm}W^{\pm})(W^{\mp}W^{\mp})$	ATLAS [132]	[0.2;0.7]	36.1
$C_8^{\ell^{\pm}\ell^{\pm}}$	$VV \to H_5^{\pm\pm} \to W^{\pm}W^{\pm}[\to (\ell^{\pm}\nu)(\ell^{\pm}\nu)]$	CMS [133]	[0.2;0.8]	19.4
$C_{13}^{\ell^{\pm}\ell^{\pm}}$	$VV \to H_5^{\pm\pm} \to W^{\pm}W^{\pm}[\to (\ell^{\pm}\nu)(\ell^{\pm}\nu)]$	CMS [134]	[0.2;1.0]	35.9

the measured h signal strengths. In Fig. 1, we show the individual impacts of specific decay categories on the α-v_Δ plane and on the plane of the relative loop couplings of h to $\gamma\gamma$ and $Z\gamma$, as well as the combination of all signal strengths. While the colored contours represent the allowed regions with 95% probability for each decay mode, the gray region gives the combined fit.

Two allowed gray regions can be seen in the left panel of Fig. 1. The bigger region close to $\alpha \approx 0°$ (corresponding to the decoupling limit of the model) shows that v_Δ cannot exceed $\approx$45 GeV, and negative α is mostly favored. The other allowed solution close to $\alpha \approx 61°$ and $v_\Delta \approx 77$ GeV is only visible as a small black dot and features a negative sign for the h couplings to vector bosons relative to the SM ($r_{ZZ} = r_{WW} = -1$). This region was not identified before as a viable possibility in the GM model (see, for instance, Ref. [17]), highlighting the advantages of using a global fitter. This region is visible only when considering the individual constraints of the h signal strengths. It disappears after taking into account the direct search results (see Fig. 3). However, if one relaxes the assumptions about the considered GM mass ranges and the direct search constraints do not apply, this may persist as a viable scenario. Compared to the parameter space in the α-v_Δ plane given in Ref. [17], the bigger allowed area here is smaller in size, as now we see that α cannot reach beyond $-25°$. This is due to the much larger data set on h signal strengths made available in the recent years as well as the addition of the $\gamma\gamma$ signal strengths.

In the right panel of Fig. 1, we show the 95% probability contours in the $r_{Z\gamma}$-$r_{\gamma\gamma}$ plane, illustrating the impact on the one-loop couplings of h to $\gamma\gamma$ and $Z\gamma$ relative to the SM. The information on the loop couplings is complementary to the tree-level couplings, which can be purely determined for a given pair of α and v_Δ from the left panel. We observe a solution around the SM values, while a much smaller h coupling to $Z\gamma$ than the SM also remains allowed, since so

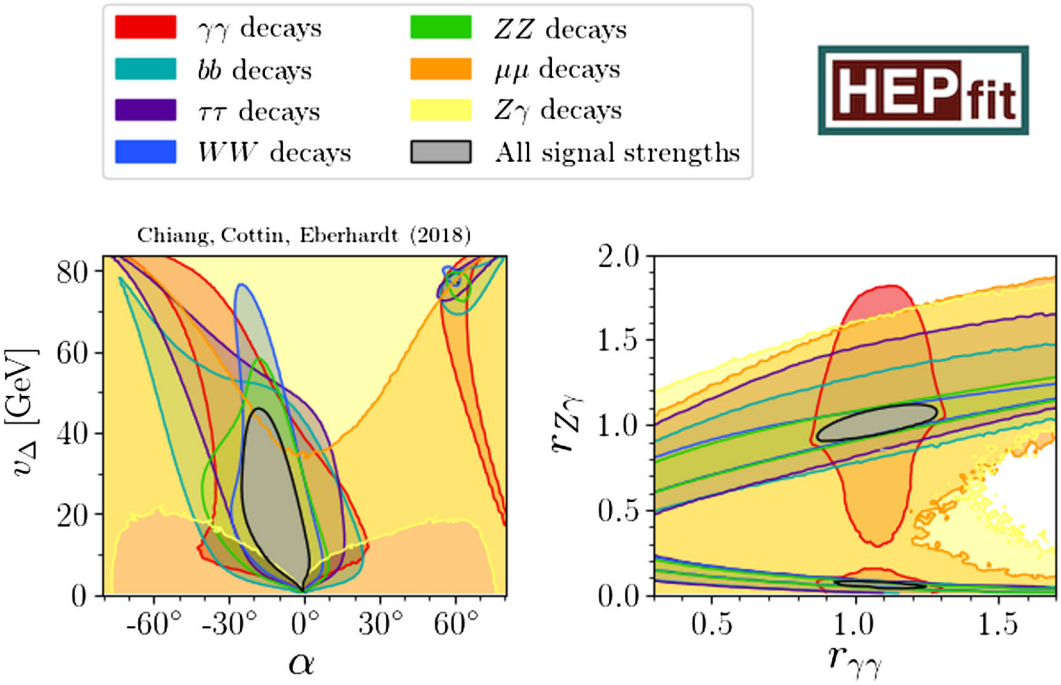

FIG. 1. Impacts of Higgs signal strengths on the v_Δ-α plane (left) and on the relative one-loop couplings of h to $\gamma\gamma$ and $Z\gamma$, $r_{\gamma\gamma}$ and $r_{Z\gamma}$, respectively (right). The 95% probability contours are shown from fits to the data for h decays to $\gamma\gamma$ (red), $Z\gamma$ (yellow), WW (blue), ZZ (green), bb (cyan), $\tau\tau$ (purple) and $\mu\mu$ (orange). The combined fit to all h signal strengths is shown in gray.

far we only have upper limits on the $Z\gamma$ signal strength. Both are mainly determined by the $\gamma\gamma$, WW and ZZ final states.

After the discussion of individual h signal strengths, we want to have a glance at the direct searches and their breakdown into searches for H_1, H_3^0, H_3^+, H_5^0, H_5^+ and H_5^{++}. In Fig. 2 we show their separate impacts on the mass-dependent 95% limits on α and v_Δ, as well as the combined fit to all of them. The angle α is only affected by the absence of H_1 signals, because the H_3 and H_5 couplings to fermions and gauge bosons do not depend on this parameter. The limits in the α-m_1 plane are rather strong for relatively small masses, sometimes even stronger than the limits from the h signal strengths, except for a small strip just above the kinematic $H_1 \to hh$ threshold. Here this channel is not constrained by the hh searches yet, and all the other branching ratios are sufficiently suppressed with respect to the hh one to weaken the search constraints from the other decays. With increasing mass, the H_1 search limits become less constraining, such that for instance for $m_1 \gtrsim 600$ GeV all negative values of α are allowed. The difference between "H_1 only" and the "all direct searches" contours can be explained by a distortion of the allowed parameter space which is more obvious in the v_Δ vs mass planes. From the m_1 dependence of the triplet VEV limit one can see that where the H_1 searches become weak, the impact of searches for $SU(2)_V$ triplet bosons takes over. A detailed insight about the contribution of neutral and charged H_3 limits can be found in the middle panels; we learn that the former are more important if $m_3 < 800$ GeV. For heavier H_3 particles, all corresponding search limits are relatively weak. The same breakdown into the impact of neutral and charged H_5 resonance searches can be found in the right panels of Fig. 2, here separately showing the roles of the singly and doubly charged search limits. While for $m_5 < 200$ GeV the experimental data on H_5 searches are not constraining at all, they yield the strongest restriction of all searches on v_Δ for quintet masses between 200 and 330 GeV, where the H_5^0 constraints are dominant. For the m_5 range from there up to 600 GeV, the three search analyses for doubly charged scalars are the most constraining. Above these mass scales all searches are more or less equally important, even if the limits on the triplet VEV are much weaker than around 250 GeV.

We want to stress that up to this point the strongest upper limit on v_Δ for $m_5 < 200$ GeV stems from H_3 searches and it is only at around 70 GeV. There seems to be a lot of parameter space left to exclude by searches for low-mass H_5 resonances (between 125 and 200 GeV), which decay to one real and one virtual gauge boson. This is a measurement that should easily be performed by the LHC experiments, and it could significantly lower the upper limit on the triplet VEV in the global fit.

We should also mention that even though our mass priors go up to 1.1 TeV in the fits, we have decided to only show the regions up to 1 TeV. This is because very close to the upper prior boundaries we observe that the contours

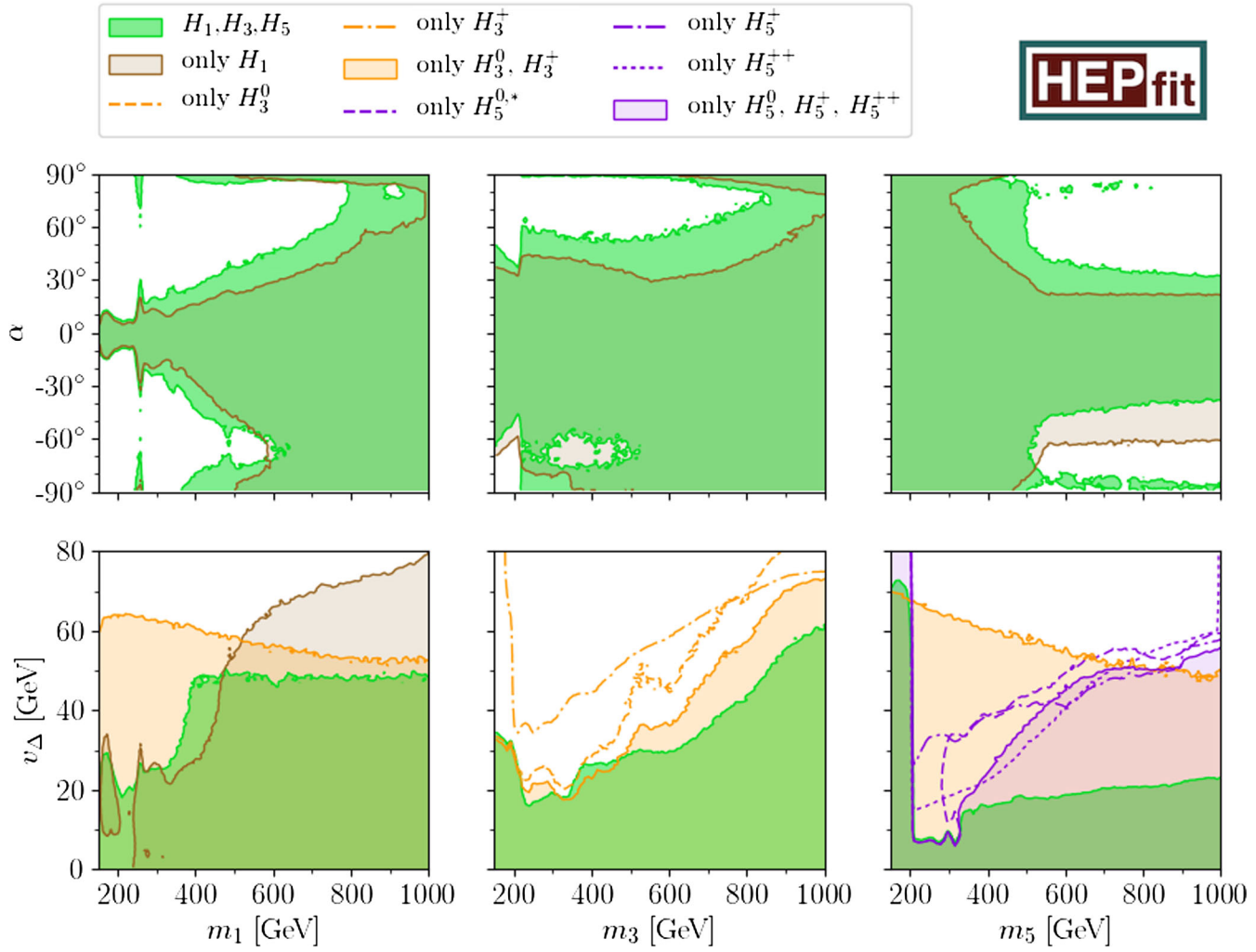

FIG. 2. Impact of different sets of direct searches on the α and v_Δ vs $m_{1,3,5}$ planes. The light brown (orange) [purple] shaded contours show the 95% allowed regions after considering only searches for H_1 (H_3) [H_5] particles. For the searches for H_3 and H_5 resonances, we show the single contributions by the neutral and singly (doubly) charged scalar search limits with the dashed and dash-dotted (dotted) lines, where the region above the lines is excluded with a probability of 95%.

become artificially small, and we do not want to confuse readers with this possibly misleading information.

Having scrutinized the h signal strengths and the absence of direct search signals individually, let us move to their combination with the theoretical bounds. In Fig. 3, we see the effects of individual sets as well as all constraints in the v_Δ-α plane (top row), the α-$m_{1,3,5}$ plane (middle row), and v_Δ-$m_{1,3,5}$ plane (bottom row). After considering all constraints, the "wrong sign" region from Fig. 1 gets excluded by the direct searches: In the middle row, we see that even if this exotic solution seems to be compatible with H_1 searches and not too far away from the regions allowed by H_3 searches, there are no red dots around $\alpha \approx 61°$ in the α-m_5 plane because all of the allowed points feature quintet masses above 1 TeV. This, however, is clearly in disagreement with the green contour stemming from all direct searches. In the combined fit including theory constraints, a rather constant region of $-25° \lesssim \alpha \lesssim 0°$ is favored across the scanned mass ranges. In the bottom row of Fig. 3, we observe the interplay of the LHC observables and the bounds imposed by positivity and unitarity. Especially in the v_Δ-m_5 plane, the contrast between the different sets of constraints becomes obvious, where a small region around $m_5 \approx 250$ GeV and $v_\Delta \approx 13$ GeV seems to be excluded by both h signal strengths and direct searches but is "resurrected" in the global combination. Also, we see in the combination that the region in which v_Δ between 30 and 40 GeV is allowed corresponds to $m_5 < 200$ GeV, where experimental improvements should be possible as mentioned above.

We note in passing that the decoupling limit [141] $(\alpha, v_\Delta \approx 0)$ is not favored by the global fit due to the choice that our mass priors only go up to 1.1 TeV.

Figure 4 shows the effect of the theory bounds, h signal strengths, direct searches and all constraints together on the mass differences of the exotic Higgs bosons in the model.

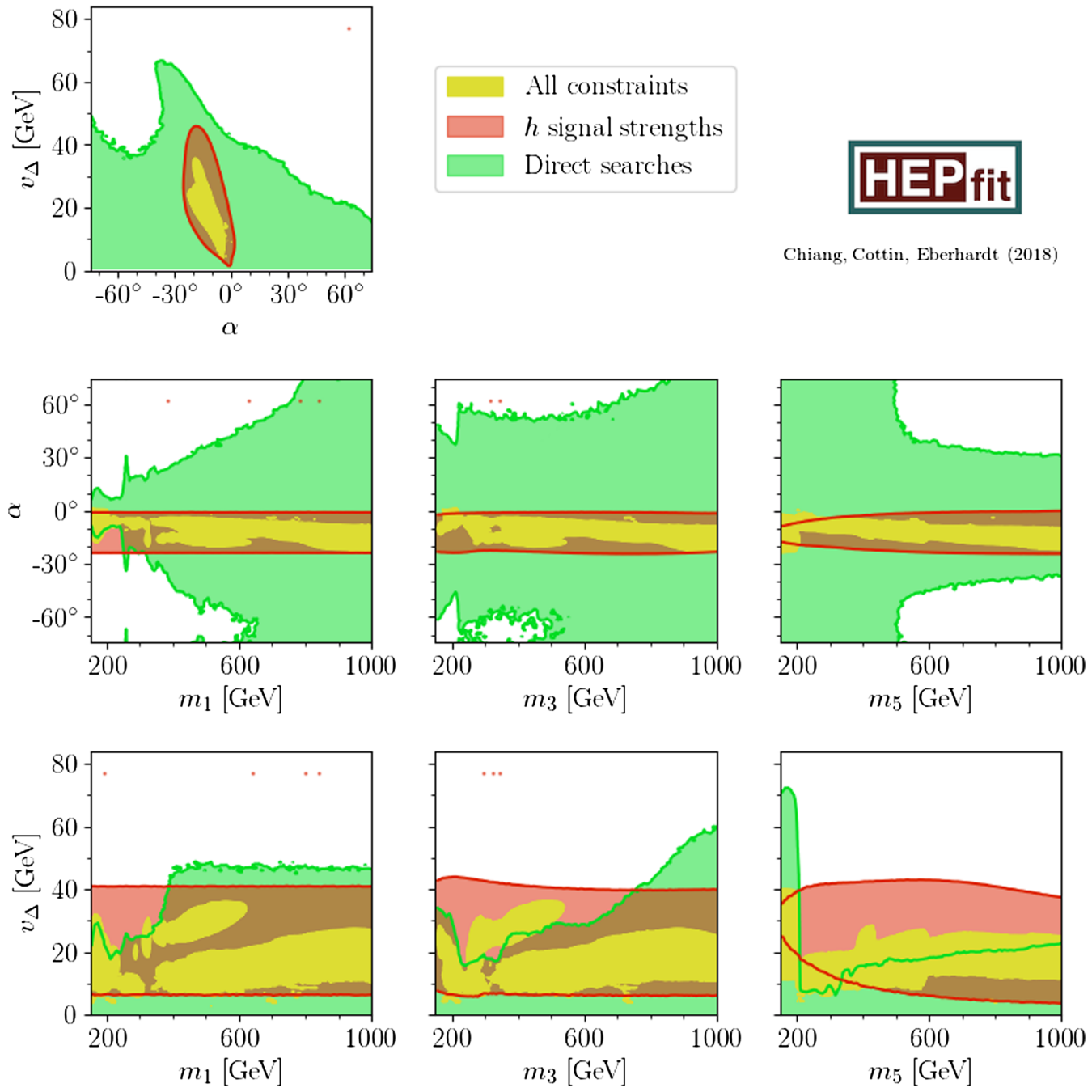

FIG. 3. Allowed 95% probability regions in the α vs v_Δ, α vs mass and v_Δ vs mass planes. The red contour shows the effect of the h signal strengths, while in green we show the impact of the direct searches. The combined fit with all constraints is shown in yellow.

Again, the colored contours represent the allowed regions with 95% probability except for the theoretical constraints, for which we assume flat likelihoods. Hence, the 95% contours would only reflect the prior shape, and the 100% contours are used for theory. Here we can see the power of the global fit: The individual sets of experimental constraints are not very strong in the $m_5 - m_1$ vs $m_3 - m_1$, $m_5 - m_3$ vs $m_3 - m_1$ and $m_5 - m_3$ vs $m_5 - m_1$ planes. The most dominant constraints come from the theoretical bounds, even though they still allow for a sizable region in the mass difference planes. However, once we combine the limits on α and v_Δ from the LHC experiments with the theoretical conditions in the global fit, the region that survives at 95% shrinks to a thin strip for $|m_3 - m_1| < 150$ GeV (the yellow region). The disjoint regions at $m_5 - m_1 \approx 250$ GeV and $m_3 - m_1 \approx 120$ GeV are a consequence of our implementation of the direct searches: Following Ref. [25], we only include on-shell decays of the

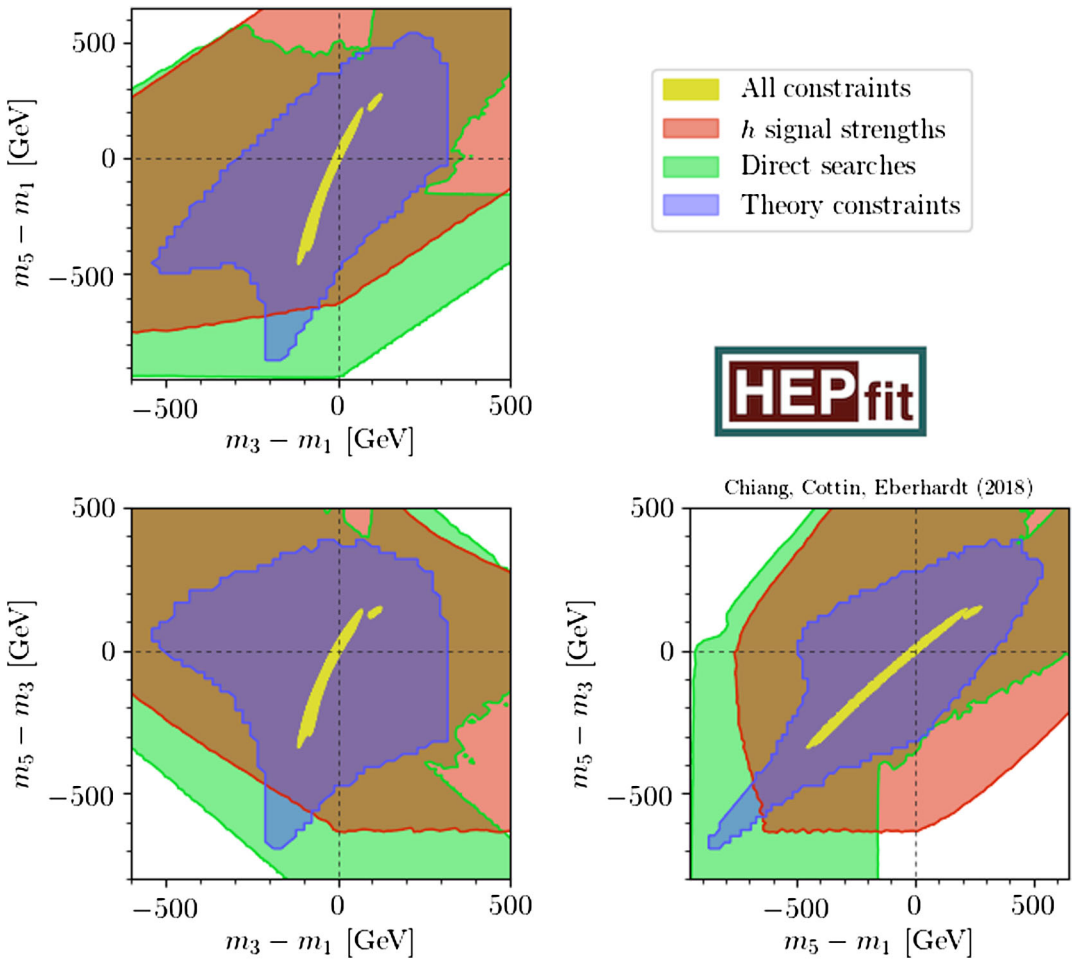

FIG. 4. Mass differences allowed at 95% probability. We show regions in the planes of $m_5 - m_1$ vs $m_3 - m_1$ (top), $m_5 - m_3$ vs $m_3 - m_1$ (bottom left) and $m_5 - m_3$ vs $m_5 - m_1$ (bottom right). Effects of the theoretical constraints, Higgs signal strengths, and direct searches are shown in blue, red, and green, respectively. The global fit with all constraints imposed is shown in yellow.

H_5 bosons. With an increasing H_5 mass, the decay to a neutral or charged H_3 and a massive vector boson can open abruptly. (The kinematic threshold is around m_W plus the minimally allowed m_3, i.e., at ∼230 GeV.) For instance, the branching ratio of $H_5^0 \to H_3^0 Z$ can jump from zero to values over 50% (see also Fig. 6). If off-shell decays were also considered, the transition for these decays would become smoother and the two regions should be connected.

After considering all the direct searches from the previous section, we find that the most powerful experimental analyses in constraining this model involve searches for the $H_{1,5}^0$ and $H_5^{\pm\pm}$ bosons. The effects of H_3^0 and $H_{3,5}^{\pm}$ observables are not as strong. In order to get more insights into our treatment of the direct searches and also to help the experimental collaborations better appreciate which search channels are more relevant or useful to the model, we show in Fig. 5 five of the most constraining searches for heavy scalar resonances implemented in this work. They include the ATLAS and CMS searches for $VV \to H_{1,5}^0 \to ZZ$ [91,92] (labeled $A_{13V}^{2\ell 2L}$ for fully leptonically decaying ZZ and A_{13V}^{2L2q} for the semileptonic final state in Table III), $pp \to H_1^0 \to hh \to bbbb$ [106,107] (labeled A_{13}^{4b} and C_{13}^{4b} in Table IV) and $VV \to H_5^{\pm\pm} \to W^{\pm}W^{\pm}$ [134] (labeled $C_{13}^{\ell^{\pm}\ell^{\pm}}$ in Table V). The gray regions in the background delimit the available GM model space if we do not apply any constraint in the fit. We show the 100% prior ranges, but also the 95% prior regions, which differ only in the $H_1 \to hh$ case by about one order of magnitude in $\sigma \cdot \mathcal{B}$. All five searches cut away a sizable portion of the allowed parameter space, ranging from a difference of less than one order of magnitude between the $H_5 \to ZZ$ search limit and the gray contour to more than 2 orders of magnitude in $\sigma \cdot \mathcal{B}$ for the searches of $H_1 \to hh$. Comparing this to the role of the individual searches in the global fit (yellow contour), we observe that the searches in the left column are not very relevant except for $m_1 < 300$ GeV, while the channels in the right column yield the strongest constraint for m_1 between 500 and 1000 GeV and for m_5 between 200 and 600 GeV, respectively. (The reason why the 95% allowed region in the last

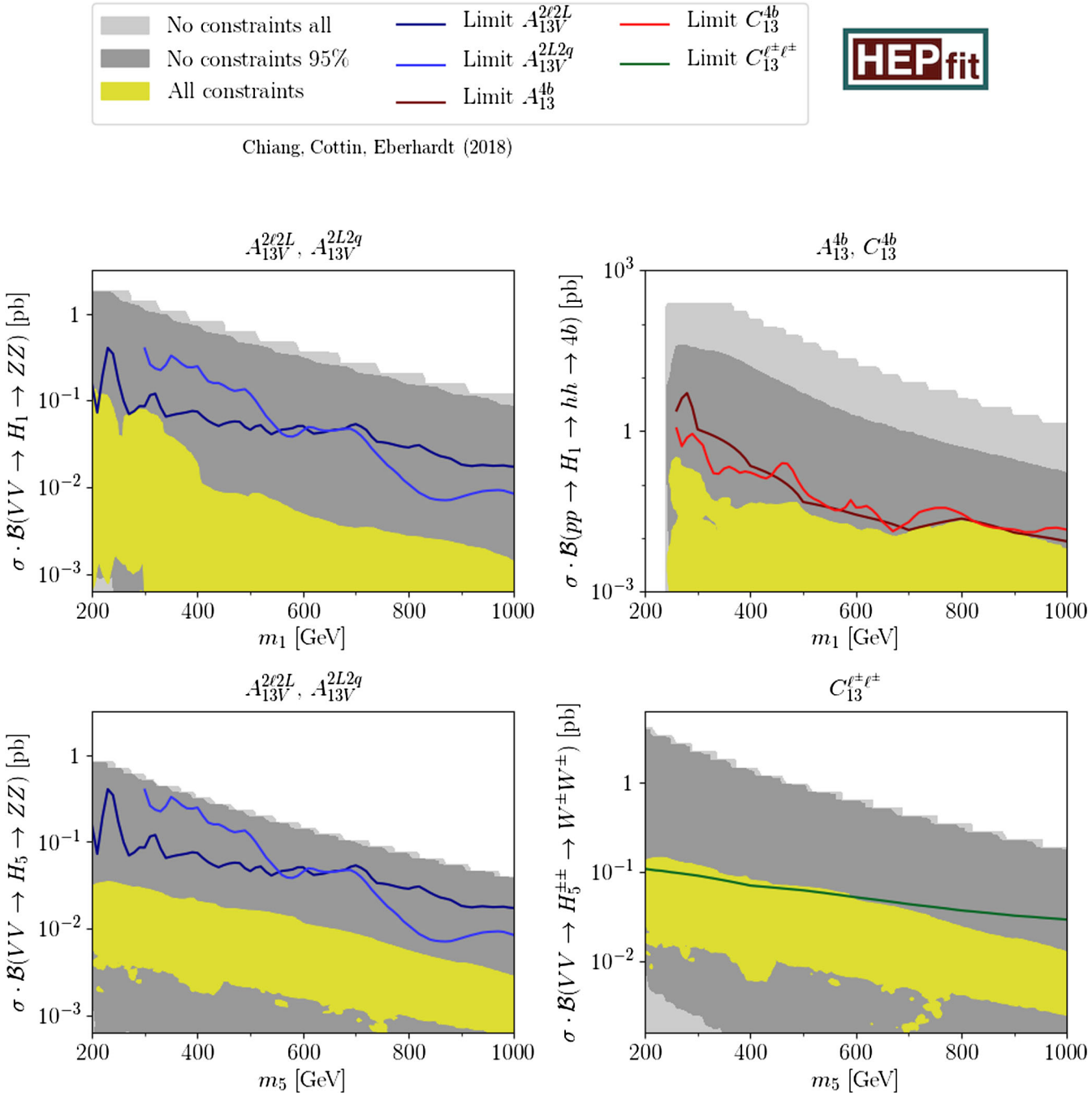

FIG. 5. Effect of five direct searches in the $\sigma \cdot \mathcal{B}$ vs mass planes. The light (dark) gray regions show the 100% (95%) prior regions. The allowed 95% probability region after considering all the constraints is shown in yellow. The blue, red and green curves denote the experimental limits on H_1 or H_5 decays to two Z bosons, on $H_1 \to hh$ and on the pair production of $H_5^{\pm\pm}$, respectively.

panel exceeds experimental exclusion limit for light H_5 can only be explained by the theoretical bounds that eliminate very low $\sigma \cdot \mathcal{B}$ values in the global fit. In the simultaneous fit to all direct searches only, the allowed contour stays below the CMS line.)

We present in Table VI the 95% probability ranges of the model parameters from our global fit. We do not get limits for the trilinear couplings μ_1 and μ_2. (More precisely, the limits that we observe in the fit are prior dependent.) The upper limit of 105 GeV on $m_1 - m_3$ enables us to exclude the decays $H_1 \to H_3^{0,+} H_3^{0,-}$, $H_1 \to H_3 Z$ as well as $H_1 \to H_3^+ W^-$ at the probability of 95%. In our fit, we also determine the 95% allowed intervals for the triple h coupling and the quartic couplings of the scalar potential. The SM value for the former is $g_{hhh}^{\mathrm{SM}} \approx -190$ GeV. In the

TABLE VI. 95% probability intervals of the GM model parameters after considering all the constraints in our fits, marginalizing over all other parameters.

Parameter	95% probability range	Parameter	95% probability range
v_Δ [GeV]$\lvert\cos\beta$	$\leq 37\rvert \leq 0.42$	λ_1	$[0.03; 0.22]$
α	$[-22°; -8°]$	λ_2	$[-0.65; 1.25]$
$m_5 - m_3$ [GeV]	$[-375; 125]$	λ_3	$[-0.9; 1.45]$
$m_5 - m_1$ [GeV]	$[-500; 225]$	λ_4	$[-0.2; 0.65]$
$m_3 - m_1$ [GeV]	$[-105; 105]$	λ_5	$[-3.0; 2.75]$
g_{hhh} [GeV]	$[-455; 50]$		

TABLE VII. 95% probability intervals of the GM model decay widths and branching ratios after considering all constraints in our fits. We only quote branching ratios larger than 5%.

H_1	95% prob. range
Γ_1	≤ 48 GeV
$\mathcal{B}(H_1^0 \to tt)$	[0;45]%
$\mathcal{B}(H_1^0 \to ZZ)$	[0;31]%
$\mathcal{B}(H_1^0 \to WW)$	[0;100]%
$\mathcal{B}(H_1^0 \to hh)$	[0;100]%
H_3	95% prob. range
Γ_3	≤ 70 GeV
$\mathcal{B}(H_3^0 \to tt)$	[0;100]%
$\mathcal{B}(H_3^0 \to hZ)$	[0;100]%
$\mathcal{B}(H_3^0 \to H_5 Z)$	[0;56]%
$\mathcal{B}(H_3^0 \to H_5^+ W^-)$	[0;100]%
Γ_{3+}	≤ 83 GeV
$\mathcal{B}(H_3^+ \to tb)$	[0;100]%
$\mathcal{B}(H_3^+ \to hW^+)$	[0;93]%
$\mathcal{B}(H_3^+ \to H_5^+ Z)$	[0;30]%
$\mathcal{B}(H_3^+ \to H_5 W^+)$	[0;11]%
$\mathcal{B}(H_3^+ \to H_5^{++} W^-)$	[0;64]%
H_5	95% prob. range
Γ_5	≤ 18 GeV
$\mathcal{B}(H_5^0 \to ZZ)$	[7;68]%
$\mathcal{B}(H_5^0 \to WW)$	[7;93]%
$\mathcal{B}(H_5^0 \to Z\gamma)$	[0;13]%
$\mathcal{B}(H_5^0 \to H_3 Z)$	[0;73]%
$\mathcal{B}(H_5^0 \to H_3^+ W^-)$	[0;40]%
Γ_{5+}	≤ 18 GeV
$\mathcal{B}(H_5^+ \to ZW^+)$	[4;100]%
$\mathcal{B}(H_5^+ \to H_3^+ Z)$	[0;46]%
$\mathcal{B}(H_5^+ \to H_3^0 W^+)$	[0;70]%
Γ_{5++}	≤ 18 GeV
$\mathcal{B}(H_5^{++} \to W^+W^+)$	[5;100]%
$\mathcal{B}(H_5^{++} \to H_3^+ W^+)$	[0;95]%

GM model, it can be enhanced by a factor of 2.4 at most, but it can be also be very small and even have the opposite sign. The quartic couplings defined in (2) are mainly constrained by unitarity and positivity. While λ_1 and λ_4 cannot be larger than 0.65 in magnitude, $|\lambda_5|$ enjoys more freedom and can even be as large as 3.0 without violating the above-mentioned theory bounds.

Limits on experimentally relevant derived quantities such as total decay widths and branching ratios for the $H_{1,3,5}$ scalars are presented in Table VII. For the total decay widths of the heavy singlet, triplet and quintet particles, we observe that they cannot exceed 48, 70 and 18 GeV, respectively. For the SM-like Higgs boson, we obtain a probability range on Γ_h between 3.9 and 4.5 MeV. In addition to the given branching ratio ranges of Table VII, we also illustrate the mass dependence of the most important branching ratios in Fig. 6. Some of the planes contain white spaces in between allowed regions [in the $\mathcal{B}(H_1 \to ZZ)$-m_1 plane, for instance, intermediate values are not completely filled at the 95% level] because it is more likely that the decay channel is completely closed or open. The branching ratio values in between would require quite some fine-tuning of the GM model parameters; nevertheless, they are not excluded. Here only the total upper and lower limits of the branching ratios and their mass dependence are important. The discussed limits on the heavy Higgs decays can serve as a guidance for the LHC experiments in the design of new searches for the scalars in the GM model.

VI. SUMMARY AND OUTLOOK

We have performed global fits in the Georgi-Machacek model for the first time, making use of the `HEPfit` package and the latest experimental data. We consider constraints from both theory (stability of the scalar potential and perturbative unitarity) and LHC Higgs observables. These include several up-to-date experimental results from run 1 and run 2 of the LHC, including all the data on Higgs boson signal strengths and 80 searches sensitive to the neutral, singly charged and doubly charged heavy Higgs particles of the Georgi-Machacek model.

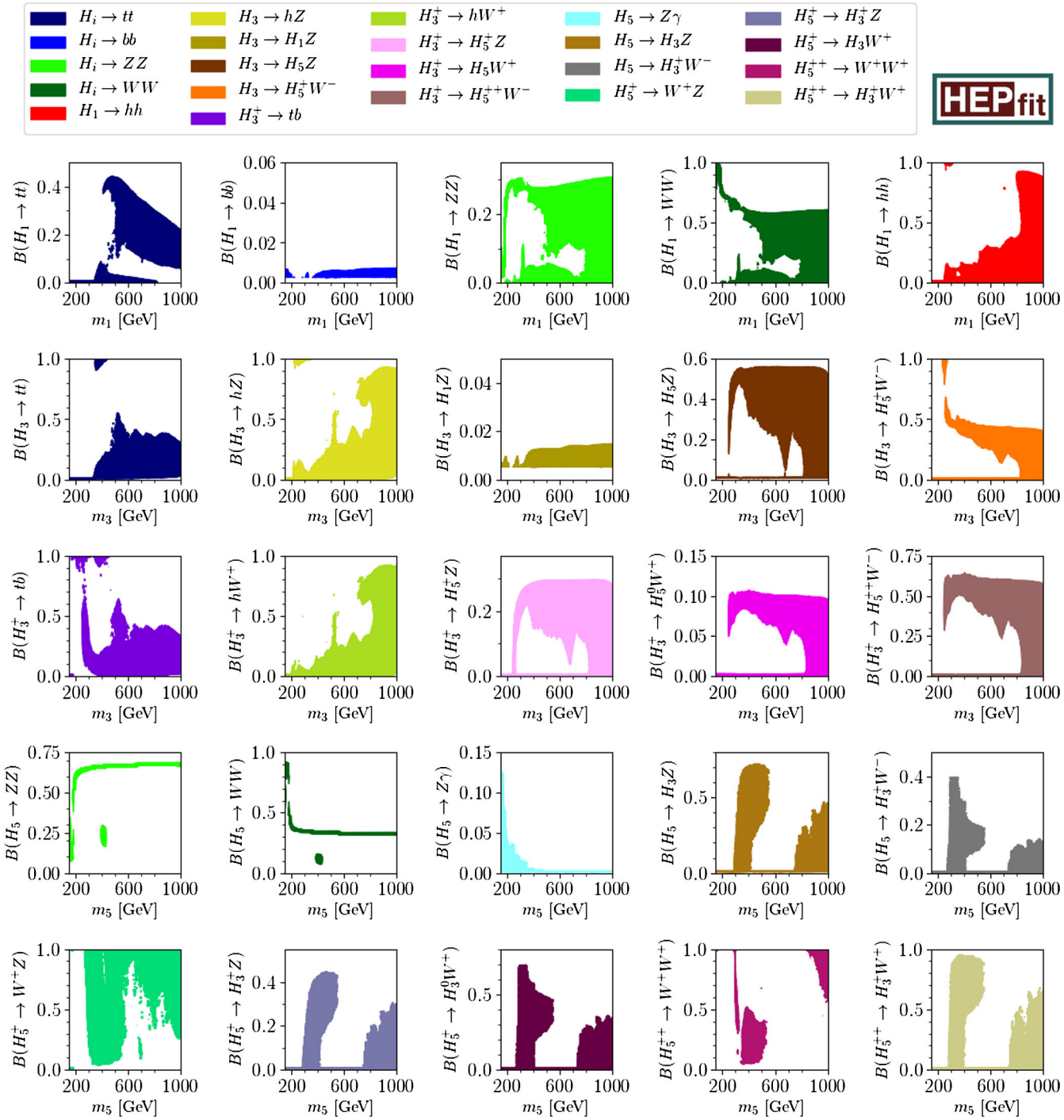

FIG. 6. 95% probability regions of the combined fit for the largest branching ratios of H_1 (top row), H_3^0 (second row), H_3^+ (third row), H_5^0 (fourth row) and charged H_5 (bottom row). Each color stands for a specific decay, and each of the neutral final states (tt, bb, ZZ and WW) shares the same color among the H_1 and H_3 and H_5 bosons.

By considering only the signal strengths for the SM-like Higgs boson, we have found a previously unexplored region in the v_Δ-α plane, featuring a negative sign in the Higgs couplings to vector bosons with respect to the SM couplings. This solution around $v_\Delta \approx 77$ GeV and $\alpha \approx 61°$ cannot be ruled out by the signal strength data alone but disappears as soon as direct search constraints are also imposed in the fit. However, with different assumptions on the masses of the heavy scalars this exotic solution might still be allowed.

The LHC searches for scalar resonances, especially the hunt for CP-even particles, constrain the vacuum expectation value of the Higgs bitriplet fields, but this upper

limit could probably even be stronger if LHC data on H_5 searches below 200 GeV were available. Inclusive LHC diphoton searches could also help constrain the Georgi-Machacek model for low mass H_5, where Drell-Yan Higgs pair production is sizable [144,145].

Combining the LHC bounds with the theory constraints in a global fit, we extract 95% probability limits on several Georgi-Machacek parameter regions and phenomenologically relevant quantities, which are significantly stronger than the bounds one would obtain when applying only one of the aforementioned sets of constraints. Among these are that α has to be between $-22°$ and $-8°$ and v_Δ smaller than 37 GeV. The latter means that $\cos\beta$ cannot exceed 0.42, which corresponds to an upper bound on $\sin\theta_H$, where the mixing angle θ_H is also used in the literature. We have found 95% limits on the differences between the heavy Higgs masses of values less than 500 GeV. The possibility of an H_1 decaying to H_3 can be excluded. We obtain upper 95% bounds on the total decay widths of the Higgs states and on many branching ratios, for the latter even mass-dependent limits. For instance, the $H_5^{\pm\pm}$ boson cannot decay into two $H_3^{\pm}$ bosons.

The existence of singly charged $H_5^{\pm}$ and doubly charged $H_5^{\pm\pm}$ scalars is a distinctive feature of the Georgi-Machacek model. Ongoing searches at the LHC (see Tables II–V) directly constrain v_Δ. Current searches for $H_5^{\pm\pm}$ producing dilepton resonances, which we did not consider in this work, could also be useful in constraining the Georgi-Machacek model in a global fit. This motivates flexibility in the definition of the experimental benchmarks in these searches to cases where the branching ratio of $H_5^{\pm\pm}$ to leptons is small, and its decay to vector bosons dominates. Other searches may also help to constrain the model when considering one-loop decays, such as the one proposed in [146] for $H^{\pm} \to W^{\pm}\gamma$.

This first global fit of the Georgi-Machacek model only represents the LHC part of the existing model constraints. Observables from flavor or electroweak precision physics could be used to further constrain the model. Also the destabilization of the custodial symmetry under renormalization group evolution is another interesting feature worthy of a detailed examination. In this context, we want to advertise the open-source `HEPfit` package that can be used to address these and other questions in comprehensive statistical analyses.

ACKNOWLEDGMENTS

The research of C.-W. C. was supported in part by the Ministry of Science and Technology (MOST) of Taiwan under Grant No. MOST-104-2628-M-002-014-MY4. G. C. acknowledges support by Grant No. MOST-106-2811-M-002-035. This work has been supported in part by the Agencia Estatal de Investigación (AEI, ES) and the European Regional Development Fund (ERDF, EU) [Grants No. FPA2014-53631-C2-1-P, No. FPA2017-84445-P and No. SEV-2014-0398]. We thank Jorge de Blas for help with the Higgs signal strength inputs and Ayan Paul for his technical support with HEPfit. We also thank Heather Logan for a discussion of our results and help with the GMcalc setup. The fits were performed on the cluster of INFN Roma Tre.

[1] ATLAS Collaboration, Observation of a new particle in the search for the Standard Model Higgs boson with the ATLAS detector at the LHC, Phys. Lett. B **716**, 1 (2012).
[2] CMS Collaboration, Observation of a new boson at a mass of 125 GeV with the CMS experiment at the LHC, Phys. Lett. B **716**, 30 (2012).
[3] C. Patrignani *et al.* (Particle Data Group), Review of particle physics, Chin. Phys. C **40**, 100001 (2016).
[4] J. Schechter and J. W. F. Valle, Neutrino masses in $SU(2) \times U(1)$ theories, Phys. Rev. D **22**, 2227 (1980).
[5] T. P. Cheng and L.-F. Li, Neutrino masses, mixings and oscillations in $SU(2) \times U(1)$ models of electroweak interactions, Phys. Rev. D **22**, 2860 (1980).
[6] H. Georgi and M. Machacek, Doubly charged Higgs bosons, Nucl. Phys. **B262**, 463 (1985).
[7] M. S. Chanowitz and M. Golden, Higgs boson triplets with $M_W = M_Z \cos\theta_W$, Phys. Lett. **165B**, 105 (1985).
[8] CMS Collaboration, Measurements of properties of the Higgs boson decaying to a W boson pair in pp collisions at $\sqrt{s} = 13$ TeV, arXiv:1806.05246.
[9] J. F. Gunion, R. Vega, and J. Wudka, Higgs triplets in the Standard Model, Phys. Rev. D **42**, 1673 (1990).
[10] C.-W. Chiang, A.-L. Kuo, and K. Yagyu, Enhancements of weak gauge boson scattering processes at the CERN LHC, J. High Energy Phys. 10 (2013) 072.
[11] C.-W. Chiang, A.-L. Kuo, and K. Yagyu, Radiative corrections to Higgs couplings with weak gauge bosons in custodial multi-Higgs models, Phys. Lett. B **774**, 119 (2017).
[12] C.-W. Chiang, A.-L. Kuo, and K. Yagyu, One-loop renormalized Higgs vertices in Georgi-Machacek model, Phys. Rev. D **98**, 013008 (2018).
[13] C.-W. Chiang and K. Yagyu, Testing the custodial symmetry in the Higgs sector of the Georgi-Machacek model, J. High Energy Phys. 01 (2013) 026.

[14] C.-W. Chiang, S. Kanemura, and K. Yagyu, Novel constraint on the parameter space of the Georgi-Machacek model with current LHC data, Phys. Rev. D **90**, 115025 (2014).
[15] C.-W. Chiang and K. Tsumura, Properties and searches of the exotic neutral Higgs bosons in the Georgi-Machacek model, J. High Energy Phys. 04 (2015) 113.
[16] H. E. Logan and V. Rentala, All the generalized Georgi-Machacek models, Phys. Rev. D **92**, 075011 (2015).
[17] C.-W. Chiang, A.-L. Kuo, and T. Yamada, Searches of exotic Higgs bosons in general mass spectra of the Georgi-Machacek model at the LHC, J. High Energy Phys. 01 (2016) 120.
[18] C. Degrande, K. Hartling, and H. E. Logan, Scalar decays to $\gamma\gamma$, $Z\gamma$, and $W\gamma$ in the Georgi-Machacek model, Phys. Rev. D **96**, 075013 (2017).
[19] H. E. Logan and M. B. Reimer, Characterizing a benchmark scenario for heavy Higgs boson searches in the Georgi-Machacek model, Phys. Rev. D **96**, 095029 (2017).
[20] HEPFit Collaboration, HEPFIT: A code for the combination of indirect and direct constrains on high energy physics models, http://hepfit.roma1.infn.it/.
[21] A. Caldwell, D. Kollar, and K. Kroninger, BAT: The Bayesian analysis toolkit, Comput. Phys. Commun. **180**, 2197 (2009).
[22] V. Cacchio, D. Chowdhury, O. Eberhardt, and C. W. Murphy, Next-to-leading order unitarity fits in two-Higgs-doublet models with soft $\mathbb{Z}_2$ breaking, J. High Energy Phys. 11 (2016) 026.
[23] D. Chowdhury and O. Eberhardt, Update of global two-Higgs-doublet model fits, J. High Energy Phys. 05 (2018) 161.
[24] O. Eberhardt, Current status of two-Higgs-doublet models with a softly broken $\mathbb{Z}_2$ symmetry, in *Proceedings of the 39th International Conference on High Energy Physics (ICHEP 2018), Seoul, 2018*, arXiv:1809.04851.
[25] K. Hartling, K. Kumar, and H. E. Logan, GMCALC: A calculator for the Georgi-Machacek model, arXiv:1412.7387.
[26] ATLAS and CMS Collaborations, Measurements of the Higgs boson production and decay rates and constraints on its couplings from a combined ATLAS and CMS analysis of the LHC pp collision data at $\sqrt{s} = 7$ and 8 TeV, J. High Energy Phys. 08 (2016) 045.
[27] J. de Blas, M. Ciuchini, E. Franco, S. Mishima, M. Pierini, L. Reina, and L. Silvestrini, Electroweak precision observables and Higgs-boson signal strengths in the Standard Model and beyond: Present and future, J. High Energy Phys. 12 (2016) 135.
[28] A. Arhrib, R. Benbrik, M. Chabab, G. Moultaka, M. C. Peyranère, L. Rahili, and J. Ramadan, The Higgs potential in the type II Seesaw model, Phys. Rev. D **84**, 095005 (2011).
[29] M. Aoki and S. Kanemura, Unitarity bounds in the Higgs model including triplet fields with custodial symmetry, Phys. Rev. D **77**, 095009 (2008).
[30] M. E. Krauss and F. Staub, Unitarity constraints in triplet extensions beyond the large s limit, Phys. Rev. D **98**, 015041 (2018).
[31] M. E. Krauss and F. Staub, Perturbativity constraints in BSM models, Eur. Phys. J. C **78**, 185 (2018).
[32] ATLAS Collaboration, Observation and measurement of Higgs boson decays to WW^* with the ATLAS detector, Phys. Rev. D **92**, 012006 (2015).
[33] CMS Collaboration, Measurement of Higgs boson production and properties in the WW decay channel with leptonic final states, J. High Energy Phys. 01 (2014) 096.
[34] ATLAS Collaboration, Evidence for the Higgs-boson Yukawa coupling to tau leptons with the ATLAS detector, J. High Energy Phys. 04 (2015) 117.
[35] CMS Collaboration, Evidence for the 125 GeV Higgs boson decaying to a pair of τ leptons, J. High Energy Phys. 05 (2014) 104.
[36] ATLAS Collaboration, Measurements of Higgs boson production and couplings in the four-lepton channel in pp collisions at center-of-mass energies of 7 and 8 TeV with the ATLAS detector, Phys. Rev. D **91**, 012006 (2015).
[37] CMS Collaboration, Precise determination of the mass of the Higgs boson and tests of compatibility of its couplings with the Standard Model predictions using proton collisions at 7 and 8 TeV, Eur. Phys. J. C **75**, 212 (2015).
[38] ATLAS Collaboration, Measurement of Higgs boson production in the diphoton decay channel in pp collisions at center-of-mass energies of 7 and 8 TeV with the ATLAS detector, Phys. Rev. D **90**, 112015 (2014).
[39] CMS Collaboration, Observation of the diphoton decay of the Higgs boson and measurement of its properties, Eur. Phys. J. C **74**, 3076 (2014).
[40] ATLAS Collaboration, Measurements of the Higgs boson production and decay rates and coupling strengths using pp collision data at $\sqrt{s} = 7$ and 8 TeV in the ATLAS experiment, Eur. Phys. J. C **76**, 6 (2016).
[41] CMS Collaboration, Search for a Higgs boson decaying into a Z and a photon in pp collisions at $\sqrt{(s)} = 7$ and 8 TeV, Phys. Lett. B **726**, 587 (2013).
[42] ATLAS Collaboration, Measurement of gluon fusion and vector boson fusion Higgs boson production cross-sections in the $H \to WW^* \to e\nu\mu\nu$ decay channel in pp collisions at $\sqrt{s} = 13$ TeV with the ATLAS detector, Technical Report No. ATLAS-CONF-2018-004, CERN, Geneva, 2018.
[43] ATLAS Collaboration, Cross-section measurements of the Higgs boson decaying to a pair of tau leptons in proton-proton collisions at $\sqrt{s} = 13$ TeV with the ATLAS detector, Technical Report No. ATLAS-CONF-2018-021, CERN, Geneva, 2018.
[44] CMS Collaboration, Observation of the Higgs boson decay to a pair of τ leptons with the CMS detector, Phys. Lett. B **779**, 283 (2018).
[45] ATLAS Collaboration, Measurements of the Higgs boson production, fiducial and differential cross sections in the 4ℓ decay channel at $\sqrt{s} = 13$ TeV with the ATLAS detector, Technical Report No. ATLAS-CONF-2018-018, CERN, Geneva, 2018.
[46] CMS Collaboration, Measurements of properties of the Higgs boson decaying into the four-lepton final state in pp collisions at $\sqrt{s} = 13$ TeV, J. High Energy Phys. 11 (2017) 047.

[47] CMS Collaboration, Measurements of properties of the Higgs boson in the four-lepton final state at $\sqrt{s} = 13$ TeV, Technical Report No. CMS-PAS-HIG-18-001, CERN, Geneva, 2018.
[48] ATLAS Collaboration, Measurements of Higgs boson properties in the diphoton decay channel using 80 fb^{-1} of pp collision data at $\sqrt{s} = 13$ TeV with the ATLAS detector, Technical Report No. ATLAS-CONF-2018-028, CERN, Geneva, 2018.
[49] CMS Collaboration, Measurements of Higgs boson properties in the diphoton decay channel in proton-proton collisions at $\sqrt{s} = 13$ TeV, arXiv:1804.02716.
[50] ATLAS Collaboration, Searches for the $Z\gamma$ decay mode of the Higgs boson and for new high-mass resonances in pp collisions at $\sqrt{s} = 13$ TeV with the ATLAS detector, J. High Energy Phys. 10 (2017) 112.
[51] CMS Collaboration, Search for the decay of a Higgs boson in the $\ell\ell\gamma$ channel in proton-proton collisions at $\sqrt{s} = 13$ TeV, J. High Energy Phys. 11 (2018) 152.
[52] ATLAS Collaboration, A search for the rare decay of the Standard Model Higgs boson to dimuons in pp collisions at $\sqrt{s} = 13$ TeV with the ATLAS Detector, Technical Report No. ATLAS-CONF-2018-026, CERN, Geneva, 2018.
[53] CMS Collaboration, Search for the Higgs boson decaying to two muons in proton-proton collisions at $\sqrt{s} = 13$ TeV, arXiv:1807.06325.
[54] ATLAS Collaboration, Search for Higgs bosons produced via vector-boson fusion and decaying into bottom quark pairs in $\sqrt{s} = 13$ TeV pp collisions with the ATLAS detector, Phys. Rev. D **98**, 052003 (2018).
[55] CMS Collaboration, Search for the Standard Model Higgs boson produced through vector boson fusion and decaying to bb with proton-proton collisions at $\sqrt(s) = 13$ TeV, Technical Report No. CMS-PAS-HIG-16-003, CERN, Geneva, 2016.
[56] ATLAS Collaboration, Search for the $b\bar{b}$ decay of the Standard Model Higgs boson in associated $(W/Z)H$ production with the ATLAS detector, J. High Energy Phys. 01 (2015) 069.
[57] CMS Collaboration, Search for the Standard Model Higgs boson produced in association with a W or a Z boson and decaying to bottom quarks, Phys. Rev. D **89**, 012003 (2014).
[58] ATLAS Collaboration, Study of $(W/Z)H$ production and Higgs boson couplings using $H \to WW^*$ decays with the ATLAS detector, J. High Energy Phys. 08 (2015) 137.
[59] ATLAS Collaboration, Observation of $H \to b\bar{b}$ decays and VH production with the ATLAS detector, Technical Report No. ATLAS-CONF-2018-036, CERN, Geneva, 2018.
[60] CMS Collaboration, Evidence for the Higgs boson decay to a bottom quark-antiquark pair, Phys. Lett. B **780**, 501 (2018).
[61] ATLAS Collaboration, Measurements of the Higgs boson production cross section via vector boson fusion and associated WH production in the $WW^* \to \ell\nu\ell\nu$ decay mode with the ATLAS detector at $\sqrt{s} = 13$ TeV, Technical Report No. ATLAS-CONF-2016-112, CERN, Geneva, 2016.
[62] CMS Collaboration, Search for the associated production of the Higgs boson and a vector boson in proton-proton collisions at $\sqrt{s} = 13$ TeV via Higgs boson decays to τ leptons, arXiv:1809.03590.
[63] ATLAS Collaboration, Search for the Standard Model Higgs boson produced in association with top quarks and decaying into $b\bar{b}$ in pp collisions at $\sqrt{s} = 8$ TeV with the ATLAS detector, Eur. Phys. J. C **75**, 349 (2015).
[64] CMS Collaboration, Search for the associated production of the Higgs boson with a top-quark pair, J. High Energy Phys. 09 (2014) 087.
[65] ATLAS Collaboration, Search for the Standard Model Higgs boson produced in association with top quarks and decaying into a $b\bar{b}$ pair in pp collisions at $\sqrt{s} = 13$ TeV with the ATLAS detector, Phys. Rev. D **97**, 072016 (2018).
[66] CMS Collaboration, Search for $t\bar{t}H$ production in the all-jet final state in proton-proton collisions at $\sqrt{s} = 13$ TeV, J. High Energy Phys. 06 (2018) 101.
[67] CMS Collaboration, Observation of $t\bar{t}H$ Production, Phys. Rev. Lett. **120**, 231801 (2018).
[68] ATLAS Collaboration, Evidence for the associated production of the Higgs boson and a top quark pair with the ATLAS detector, Phys. Rev. D **97**, 072003 (2018).
[69] CMS Collaboration, Evidence for associated production of a Higgs boson with a top quark pair in final states with electrons, muons, and hadronically decaying τ leptons at $\sqrt{s} = 13$ TeV, J. High Energy Phys. 08 (2018) 066.
[70] T. Aaltonen *et al.* (CDF Collaboration), Combination for searches for the Higgs boson using the full CDF data set, Phys. Rev. D **88**, 052013 (2013).
[71] V. M. Abazov *et al.* (D0 Collaboration), Combined search for the Higgs boson with the D0 experiment, Phys. Rev. D **88**, 052011 (2013).
[72] J. de Blas, O. Eberhardt, and C. Krause, Current and future constraints on Higgs couplings in the nonlinear effective theory, J. High Energy Phys. 07 (2018) 048.
[73] ATLAS Collaboration, Search for new phenomena in events with same-charge leptons and b-jets in pp collisions at $\sqrt{s} = 13$ TeV with the ATLAS detector, arXiv:1807.11883.
[74] ATLAS Collaboration, Search for new phenomena in $t\bar{t}$ final states with additional heavy-flavour jets in pp collisions at $\sqrt{s} = 13$ TeV with the ATLAS detector, Technical Report No. ATLAS-CONF-2016-104, CERN, Geneva, 2016.
[75] CMS Collaboration, Search for neutral MSSM Higgs bosons decaying into a pair of bottom quarks, J. High Energy Phys. 11 (2015) 071.
[76] CMS Collaboration, Search for Narrow Resonances in the b-Tagged Dijet Mass Spectrum in Proton-Proton Collisions at $\sqrt{s} = 8$ TeV, Phys. Rev. Lett. **120**, 201801 (2018).
[77] CMS Collaboration, Search for a narrow heavy decaying to bottom quark pairs in the 13 TeV data sample, Technical Report No. CMS-PAS-HIG-16-025, CERN, Geneva, 2016.
[78] CMS Collaboration, Search for beyond the Standard Model Higgs bosons decaying into a $b\bar{b}$ pair in pp collisions at $\sqrt{s} = 13$ TeV, J. High Energy Phys. 08 (2018) 113.
[79] ATLAS Collaboration, Search for neutral Higgs bosons of the minimal supersymmetric Standard Model in pp

collisions at $\sqrt{s} = 8$ TeV with the ATLAS detector, J. High Energy Phys. 11 (2014) 056.
[80] CMS Collaboration, Search for additional neutral Higgs bosons decaying to a pair of tau leptons in pp collisions at $\sqrt{s} = 7$ and 8 TeV, Technical Report No. CMS-PAS-HIG-14-029, CERN, Geneva, 2015.
[81] ATLAS Collaboration, Search for additional heavy neutral Higgs and gauge bosons in the ditau final state produced in 36 fb^{-1} of pp collisions at $\sqrt{s} = 13$ TeV with the ATLAS detector, J. High Energy Phys. 01 (2018) 055.
[82] CMS Collaboration, Search for additional neutral MSSM Higgs bosons in the $\tau\tau$ final state in proton-proton collisions at $\sqrt{s} = 13$ TeV, J. High Energy Phys. 09 (2018) 007.
[83] ATLAS Collaboration, Search for Scalar Diphoton Resonances in the Mass Range 65–600 GeV with the ATLAS Detector in pp Collision Data at $\sqrt{s} = 8$ TeV, Phys. Rev. Lett. **113**, 171801 (2014).
[84] ATLAS Collaboration, Search for new phenomena in high-mass diphoton final states using 37 fb^{-1} of proton-proton collisions collected at $\sqrt{s} = 13$ TeV with the ATLAS detector, Phys. Lett. B **775**, 105 (2017).
[85] CMS Collaboration, Search for high-mass diphoton resonances in proton-proton collisions at 13 TeV and combination with 8 TeV search, Phys. Lett. B **767**, 147 (2017).
[86] ATLAS Collaboration, Search for new resonances in $W\gamma$ and $Z\gamma$ final states in pp collisions at $\sqrt{s} = 8$ TeV with the ATLAS detector, Phys. Lett. B **738**, 428 (2014).
[87] CMS Collaboration, Search for scalar resonances in the 200–1200 GeV mass range decaying into a Z and a photon in pp collisions at $\sqrt{s} = 8$ TeV, Technical Report No. CMS-PAS-HIG-16-014, CERN, Geneva, 2016.
[88] ATLAS Collaboration, Search for heavy resonances decaying to a photon and a hadronically decaying $Z/W/H$ boson in pp collisions at $\sqrt{s} = 13$ TeV with the ATLAS detector, Phys. Rev. D **98**, 032015 (2018).
[89] CMS Collaboration, Search for $Z\gamma$ resonances using leptonic and hadronic final states in proton-proton collisions at $\sqrt{s} = 13$ TeV, J. High Energy Phys. 09 (2018) 148.
[90] ATLAS Collaboration, Search for an additional, heavy Higgs boson in the $H \to ZZ$ decay channel at $\sqrt{s} = 8$ TeV in pp collision data with the ATLAS detector, Eur. Phys. J. C **76**, 45 (2016).
[91] ATLAS Collaboration, Search for heavy ZZ resonances in the $\ell^+\ell^-\ell^+\ell^-$ and $\ell^+\ell^-\nu\bar{\nu}$ final states using proton-proton collisions at $\sqrt{s} = 13$ TeV with the ATLAS detector, Eur. Phys. J. C **78**, 293 (2018).
[92] ATLAS Collaboration, Searches for heavy ZZ and ZW resonances in the $\ell\ell qq$ and $\nu\nu qq$ final states in pp collisions at $\sqrt{s} = 13$ TeV with the ATLAS detector, J. High Energy Phys. 03 (2018) 009.
[93] CMS Collaboration, Search for a new scalar resonance decaying to a pair of Z bosons in proton-proton collisions at $\sqrt{s} = 13$ TeV, J. High Energy Phys. 03 (2018) 009.
[94] CMS Collaboration, Search for a heavy resonance decaying into a Z boson and a vector boson in the $\nu\bar{\nu}q\bar{q}$ final state, J. High Energy Phys. 07 (2018) 075.
[95] ATLAS Collaboration, Search for a high-mass Higgs boson decaying to a W boson pair in pp collisions at $\sqrt{s} = 8$ TeV with the ATLAS detector, J. High Energy Phys. 01 (2016) 032.
[96] ATLAS Collaboration, Search for heavy resonances decaying into WW in the $e\nu\mu\nu$ final state in pp collisions at $\sqrt{s} = 13$ TeV with the ATLAS detector, Eur. Phys. J. C **78**, 24 (2018).
[97] CMS Collaboration, Search for high mass Higgs to WW with fully leptonic decays using 2015 data, Technical Report No. CMS-PAS-HIG-16-023, CERN, Geneva, 2016.
[98] ATLAS Collaboration, Search for WW/WZ resonance production in $\ell\nu qq$ final states in pp collisions at $\sqrt{s} =$ 13 TeV with the ATLAS detector, J. High Energy Phys. 03 (2018) 042.
[99] CMS Collaboration, Search for a heavy resonance decaying to a pair of vector bosons in the lepton plus merged jet final state at $\sqrt{s} = 13$ TeV, J. High Energy Phys. 05 (2018) 088.
[100] CMS Collaboration, Search for a Higgs boson in the mass range from 145 to 1000 GeV decaying to a pair of W or Z bosons, J. High Energy Phys. 10 (2015) 144.
[101] ATLAS Collaboration, Searches for Higgs boson pair production in the $hh \to bb\tau\tau, \gamma\gamma WW^*, \gamma\gamma bb, bbbb$ channels with the ATLAS detector, Phys. Rev. D **92**, 092004 (2015).
[102] CMS Collaboration, Search for resonant pair production of Higgs bosons decaying to two bottom quark-antiquark pairs in proton-proton collisions at 8 TeV, Phys. Lett. B **749**, 560 (2015).
[103] CMS Collaboration, Search for two Higgs bosons in final states containing two photons and two bottom quarks in proton-proton collisions at 8 TeV, Phys. Rev. D **94**, 052012 (2016).
[104] CMS Collaboration, Searches for a heavy scalar boson H decaying to a pair of 125 GeV Higgs bosons hh or for a heavy pseudoscalar boson A decaying to Zh, in the final states with $h \to \tau\tau$, Phys. Lett. B **755**, 217 (2016).
[105] CMS Collaboration, Search for Higgs boson pair production in the $bb\tau\tau$ final state in proton-proton collisions at $\sqrt{(s)} = 8$ TeV, Phys. Rev. D **96**, 072004 (2017).
[106] ATLAS Collaboration, Search for pair production of Higgs bosons in the $b\bar{b}b\bar{b}$ final state using proton-proton collisions at $\sqrt{s} = 13$ TeV with the ATLAS detector, arXiv:1804.06174.
[107] CMS Collaboration, Search for resonant pair production of Higgs bosons decaying to bottom quark-antiquark pairs in proton-proton collisions at 13 TeV, J. High Energy Phys. 08 (2018) 152.
[108] ATLAS Collaboration, Search for Higgs boson pair production in the $\gamma\gamma b\bar{b}$ final state with 13 TeV pp collision data collected by the ATLAS experiment, J. High Energy Phys. 11 (2018) 040.
[109] CMS Collaboration, Search for Higgs boson pair production in the $\gamma\gamma b\bar{b}$ final state in pp collisions at $\sqrt{s} = 13$ TeV, arXiv:1806.00408.
[110] ATLAS Collaboration, A Search for Resonant and Nonresonant Higgs Boson Pair Production in the $b\bar{b}\tau^+\tau^-$ Decay Channel in pp Collisions at $\sqrt{s} = 13$ TeV with the ATLAS Detector, Phys. Rev. Lett. **121**, 191801 (2018).

[111] CMS Collaboration, Search for Higgs boson pair production in events with two bottom quarks and two tau leptons in proton-proton collisions at $\sqrt{s} = 13$ TeV, Phys. Lett. B **778**, 101 (2018).
[112] CMS Collaboration, Search for heavy resonances decaying into two Higgs bosons or into a Higgs boson and a W or Z boson in proton-proton collisions at 13 TeV, arXiv:1808.01365.
[113] CMS Collaboration, Search for resonant and nonresonant Higgs boson pair production in the bblnulnu final state in proton-proton collisions at $\sqrt{(s)} = 13$ TeV, J. High Energy Phys. 01 (2018) 054.
[114] ATLAS Collaboration, Search for Higgs boson pair production in the $\gamma\gamma WW^*$ channel using pp collision data recorded at $\sqrt{s} = 13$ TeV with the ATLAS detector, arXiv:1807.08567.
[115] ATLAS Collaboration, Search for a CP-odd Higgs boson decaying to Zh in pp collisions at $\sqrt{s} = 8$ TeV with the ATLAS detector, Phys. Lett. B **744**, 163 (2015).
[116] CMS Collaboration, Search for a pseudoscalar boson decaying into a Z boson and the 125 GeV Higgs boson in $\ell^+\ell^- b\bar{b}$ final states, Phys. Lett. B **748**, 221 (2015).
[117] ATLAS Collaboration, Search for heavy resonances decaying into a W or Z boson and a Higgs boson in final states with leptons and b-jets in 36 fb^{-1} of $\sqrt{s} = 13$ TeV pp collisions with the ATLAS detector, J. High Energy Phys. 03 (2018) 174.
[118] CMS Collaboration, Search for a heavy pseudoscalar boson decaying to a Z boson and a Higgs boson at $\sqrt{(s)} = 13$ TeV, Technical Report No. CMS-PAS-HIG-18-005, CERN, Geneva, 2018.
[119] CMS Collaboration, Search for heavy resonances decaying into a vector boson and a Higgs boson in final states with charged leptons, neutrinos and b quarks at $\sqrt{s} = 13$ TeV, arXiv:1807.02826.
[120] CMS Collaboration, Search for neutral resonances decaying into a Z boson and a pair of b jets or τ leptons, Phys. Lett. B **759**, 369 (2016).
[121] ATLAS Collaboration, Search for a heavy Higgs boson decaying into a Z boson and another heavy Higgs boson in the $\ell\ell bb$ final state in pp collisions at $\sqrt{s} = 13$ TeV with the ATLAS detector, Phys. Lett. B **783**, 392 (2018).
[122] ATLAS Collaboration, Search for charged Higgs bosons decaying via $H^\pm \to \tau^\pm\nu$ in fully hadronic final states using pp collision data at $\sqrt{s} = 8$ TeV with the ATLAS detector, J. High Energy Phys. 03 (2015) 088.
[123] CMS Collaboration, Search for a charged Higgs boson in pp collisions at $\sqrt{s} = 8$ TeV, J. High Energy Phys. 11 (2015) 018.
[124] ATLAS Collaboration, Search for charged Higgs bosons decaying via $H^\pm \to \tau^\pm\nu_\tau$ in the $\tau +$ jets and τ+lepton final states with 36 fb^{-1} of pp collision data recorded at $\sqrt{s} = 13$ TeV with the ATLAS experiment, J. High Energy Phys. 09 (2018) 139.
[125] CMS Collaboration, Search for charged Higgs bosons with the $H^\pm \to \tau^\pm\nu_\tau$ decay channel in the fully hadronic final state at $\sqrt{s} = 13$ TeV, Technical Report No. CMS-PAS-HIG-16-031, CERN, Geneva, 2016.
[126] ATLAS Collaboration, Search for charged Higgs bosons in the $H^\pm \to tb$ decay channel in pp collisions at $\sqrt{s} = 8$ TeV using the ATLAS detector, J. High Energy Phys. 03 (2016) 127.
[127] ATLAS Collaboration, Search for charged Higgs bosons decaying into top and bottom quarks at $\sqrt{s} = 13$ TeV with the ATLAS detector, J. High Energy Phys. 11 (2018) 085.
[128] ATLAS Collaboration, Search for a Charged Higgs Boson Produced in the Vector-Boson Fusion Mode with Decay $H^\pm \to W^\pm Z$ using pp Collisions at $\sqrt{s} = 8$ TeV with the ATLAS Experiment, Phys. Rev. Lett. **114**, 231801 (2015).
[129] ATLAS Collaboration, Search for resonant WZ production in the fully leptonic final state in proton-proton collisions at $\sqrt{s} = 13$ TeV with the ATLAS detector, Phys. Lett. B **787**, 68 (2018).
[130] CMS Collaboration, Search for Charged Higgs Bosons Produced via Vector Boson Fusion and Decaying into a Pair of W and Z Bosons Using pp Collisions at $\sqrt{s} = 13$ TeV, Phys. Rev. Lett. **119**, 141802 (2017).
[131] CMS Collaboration, Measurement of electroweak WZ production and search for new physics in pp collisions at $\sqrt{(s)} = 13$ TeV, Technical Report No. CMS-PAS-SMP-18-001, CERN, Geneva, 2018.
[132] ATLAS Collaboration, Search for doubly charged scalar bosons decaying into same-sign W boson pairs with the ATLAS detector, arXiv:1808.01899.
[133] CMS Collaboration, Study of Vector Boson Scattering and Search for New Physics in Events with Two Same-Sign Leptons and Two Jets, Phys. Rev. Lett. **114**, 051801 (2015).
[134] CMS Collaboration, Observation of Electroweak Production of Same-Sign W Boson Pairs in the Two Jet and Two Same-Sign Lepton Final State in Proton-Proton Collisions at $\sqrt{s} = 13$ TeV, Phys. Rev. Lett. **120**, 081801 (2018).
[135] CMS Collaboration, A search for a doubly-charged Higgs boson in pp collisions at $\sqrt{s} = 7$ TeV, Eur. Phys. J. C **72**, 2189 (2012).
[136] CMS Collaboration, Search for a doubly-charged Higgs boson with $\sqrt{s} = 8$ TeV pp collisions at the CMS experiment, Technical Report No. CMS-PAS-HIG-14-039, CERN, Geneva, 2016.
[137] CMS Collaboration, A search for doubly-charged Higgs boson production in three and four lepton final states at $\sqrt{s} = 13$ TeV, Technical Report No. CMS-PAS-HIG-16-036, CERN, Geneva, 2017.
[138] ATLAS Collaboration, Search for anomalous production of prompt same-sign lepton pairs and pair-produced doubly charged Higgs bosons with $\sqrt{s} = 8$ TeV pp collisions using the ATLAS detector, J. High Energy Phys. 03 (2015) 041.
[139] ATLAS Collaboration, Search for doubly charged Higgs boson production in multi-lepton final states with the ATLAS detector using proton-proton collisions at $\sqrt{s} = 13$ TeV, Eur. Phys. J. C **78**, 199 (2018).
[140] S. Kanemura, M. Kikuchi, H. Yokoya, and K. Yagyu, LHC run-I constraint on the mass of doubly charged Higgs bosons in the same-sign diboson decay scenario, Prog. Theor. Exp. Phys. **2015**, 51B02 (2015).
[141] K. Hartling, K. Kumar, and H. E. Logan, The decoupling limit in the Georgi-Machacek model, Phys. Rev. D **90**, 015007 (2014).

[142] LHC Higgs cross section working group Collaboration Web page, https://twiki.cern.ch/twiki/bin/view/LHCPhysics/LHCHXSWG.

[143] J. Alwall, R. Frederix, S. Frixione, V. Hirschi, F. Maltoni, O. Mattelaer, H.-S. Shao, T. Stelzer, P. Torrielli, and M. Zaro, The automated computation of tree-level and next-to-leading order differential cross sections, and their matching to parton shower simulations, J. High Energy Phys. 07 (2014) 079.

[144] R. Vega, R. Vega-Morales, and K. Xie, Light (and darkness) from a light hidden Higgs, J. High Energy Phys. 06 (2018) 137.

[145] A. Delgado, M. Garcia-Pepin, M. Quiros, J. Santiago, and R. Vega-Morales, Diphoton and diboson probes of fermiophobic Higgs bosons at the LHC, J. High Energy Phys. 06 (2016) 042.

[146] H. E. Logan and Y. Wu, Searching for the $W\gamma$ decay of a charged Higgs boson, J. High Energy Phys. 11 (2018) 121.